Ordering Kinetics and Alignment of Block Copolymer Lamellae under Shear Flow

H. Wang, M. C. Newstein, A. Krishnan, N. P. Balsara,* and B. A. Garetz*

Departments of Chemical Engineering, Chemistry, Materials Science, and Electrical Engineering, Polytechnic University, Six Metrotech Center, Brooklyn, New York 11201

B. Hammouda

National Institute of Standards and Technology, Building 235, E151, Gaithersburg, Maryland 20899

R. Krishnamoorti

Department of Chemical Engineering, University of Houston, 4800 Calhoun, Houston, Texas 77204

Received August 3, 1998; Revised Manuscript Received December 21, 1998

ABSTRACT: The effect of large-amplitude oscillatory shear flow on a concentrated block copolymer solution with lamellar order was studied by in-situ small-angle neutron scattering. Microstructural changes were studied as a function of temperature, frequency of the oscillatory flow field, and thermal history prior to turning on the shear field. We find that the alignment path depends mainly on thermal history prior to turning on the shear field and is independent of frequency and temperature. At long times, the lamellae were aligned parallel to the shearing plates, regardless of frequency, temperature, and thermal history. We refer to this as the parallel orientation. Monotonic changes from the unaligned to the aligned state were found when the shear field was turned on after the sample was completely ordered. The alignment kinetics, in this case, occurs in two stages. The first stage consists of a rapid rotation of the grains so that the lamellar normals lie in the velocity gradient−vorticity plane. This is followed by a slower process wherein the lamellar normals get increasingly localized in the velocity gradient direction. We also studied ordering kinetics under shear, by turning on the shear field before significant ordering had taken place. In this case, the first stage of ordering resulted in the formation of lamellae aligned perpendicular to the shearing plates in addition to the parallel lamellae, regardless of temperature and frequency. Eventually the perpendicular lamellae were transformed to parallel lamellae via an undulation instability.

Introduction

Block and graft copolymers are important components in a variety of microstructured materials such as adhesives, thermoplastic elastomers, and compatibilized polymer blends.[1] Traditional methods used to manufacture these materials often lead to polydisperse morphologies. The lack of precise control over microstructure is probably unimportant for current applications because these materials are used in applications that rely on their mechanical properties such as impact strength and damping coefficient. Microstructure is only important insofar as its effect on these properties. In contrast, recent efforts to use block copolymers in electronic and photonic applications require the production of highly ordered, defect-free materials.[2,3] The microstructure plays an active role in these applications, and precise morphological control is essential. While ordered microstructures can be obtained from anionically synthesized block copolymers,[4] the processing steps that are necessary to obtain defect-free materials have not been firmly established.

Block copolymers exhibit an order-to-disorder transition under quiescent conditions. A schematic view of the disordered and ordered states is shown in Figure 1 (parts a and b). In this paper, we focus on block copolymer systems with lamellar order. The ordered state obtained under quiescent conditions consists of randomly oriented grains with concomitant defects. The elimination of defects in block copolymers by the imposition of shear flow has been investigated by a number of researchers.[5−22] These studies have shown that the flow-induced microstructure in block copolymers depends on a number of experimental variables such as shear rate, molecular architecture, and thermal history prior to turning on the shear field. In some cases, highly ordered, "single crystals" are obtained under shear flow (e.g., refs 5−12 and 18). In other cases, the microstructure is destroyed by the imposition of shear flow (e.g., refs 14, 17, 19, and 22). Koppi et al. studied the alignment of polyolefin block copolymer lamellae as a function of temperature and shear rate.[7] They found that the shear rate−temperature plane could be divided into two regions: one where the lamellae were oriented

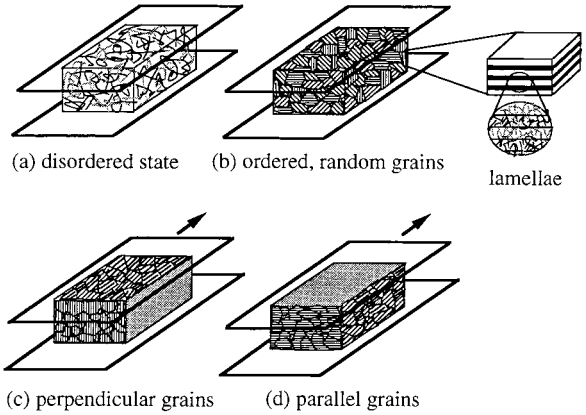

Figure 1. Microstructures of symmetric diblock copolymers.

10.1021/ma981226d CCC: $18.00
Published on Web 05/13/1999

parallel to the shearing plates and the other where the lamellae were oriented perpendicular to the shearing plates. Following Koppi et al., we refer to these orientations as parallel and perpendicular, respectively. Subsequent work has led to the construction of similar "orientation maps" for a number of different block copolymer systems.[8−12,14,16,19] A schematic view of shear-aligned block copolymer lamellae are shown in Figure 1 (parts c and d).

The results of shear-induced microstructural transitions are often represented by "phase diagrams", as opposed to orientation maps. One may question the use of this terminology, because these are nonequilibrium systems that must dissipate heat in order to maintain constant temperature under flow, while the conventional usage of the term phase diagram implies equilibrium. Nevertheless, theoretical and experimental results on sheared colloidal suspensions[23,24] and low molecular weight liquid crystals[25,26] are accurately represented by phase diagrams because the shear-induced microstructural transitions are reversible, and the state of these sheared systems is independent of history. Likewise, the phenomenon of shear-induced ordering in block copolymers that are subjected to shear flow above the quiescent disorder−order transition can be described by phase diagrams.[12,20,22,28−30] In contrast, all the results obtained by shearing block copolymers below the quiescent disorder−order transition exhibit irreversibility and history dependence.[7−11,17] For example, Koppi et al. reported that once perpendicular lamellae were obtained, switching temperature and/or shear rate into the parallel region of the orientation map did not result in a change in lamellar orientation.[7] Zhang et al. report that lamellar orientations in a block copolymer melt depended on the nature of the thermal quench from the disordered to the ordered state, prior to turning on the shear field.[11] Thus, they were able to obtain different orientations at a given temperature and shear rate, depending on whether the sample was quenched or annealed. These examples[7,11] clearly demonstrate that lamellar orientation is a path variable and not a state variable. Current theories on shear-induced orientation in block copolymers[31,32] do not address path dependence or irreversibility.

The pathways of lamellar alignment have been studied by in-situ structural probes such as small-angle neutron scattering[12,16,17−22] and flow birefringence.[9,10] In most cases, a monotonic change from an unaligned structure to an aligned structure was found. Gupta et al. were the first to report nonmonotonic changes in lamellar alignment using flow birefringence,[9] electron microscopy, and X-ray scattering.[10] They found a temperature−frequency window in which the structure alignment in a block copolymer melt changed first from isotropic to perpendicular and then from perpendicular to parallel. In another study,[19] it was found that the structure in a concentrated block copolymer solution changed first from isotropic to perpendicular and then from perpendicular to disorder. In this case,[19] instead of eliminating defects, the application of shear flow results in the elimination of the structure itself.

At this juncture, it appears that alignment kinetics and final orientations of block copolymer lamellae under shear flow depend unpredictably on a large number of experimental variables. Given the nonmonotonic nature of the alignment kinetics, one may also suspect that many "final" orientations that have been reported may, in fact, be long-lived intermediate states. It is appropriate to note that many aspects of ordering kinetics under quiescent conditions are not understood at the present time. In a recent study[33−35] it was shown that the time required for the completion of the disorder-to-order transition, at modest quench depths between 3 and 10 °C, was 500−1000 min. In this system, the time scale of ordering kinetics was 2 orders of magnitude longer than the molecular relaxation time, measured by rheology. In another study, Hajduk et al. report that under quiescent conditions several days of annealing is not sufficient for completing microstructural transformations from one ordered state to another.[36] It would therefore not be surprising if the time scales for microstructural changes in block copolymers under flow are considerably longer than typical shear alignment experiments.

In an attempt to identify the important parameters that control lamellar alignment kinetics and to avoid long-lived intermediate states, we prepared a 51 wt % solution of a polystyrene-*block*-polyisoprene copolymer in dioctyl phthalate. The viscosity of the material is relatively low (less than 10^4 P in the disordered state, 1 °C above the disorder−order transition). Estimates of molecular relaxation time at the temperatures of interest ranged from 0.1 to 1 s.[37] Our shear alignment experiments lasted for about 100 min, thus covering a time window that is 3−4 orders of magnitude longer than the molecular relaxation time. We focus on three parameters: shear rate, temperature, and thermal history prior. The feature that distinguishes this work from previous studies (including earlier work published by our group) is that we present a quantitative characterization of the system prior to turning on the shear field. We find that the alignment path depends only on the state of the system prior to turning on the shear field and is independent of shear rate and temperature.

We used two strategies (thermal histories) to obtain shear aligned samples starting from the disordered state. In the first strategy, the shear flow was turned on as soon as the sample temperature had equilibrated, after a thermal quench from the disordered to the ordered state. The fraction of ordered material in the sample at this point was negligible. Due to the fact that the *s*hear flow was imposed on a *d*isordered material, we refer to this strategy as SD. In the second strategy, the sample was held quiescently in the ordered state until the ordering was completed, before turning on the shear field. In this case, the *s*hear flow acts on an *o*rdered phase, and we refer to this strategy as SO. Depolarized light scattering experiments were carried out to determine the microstructure of the sample prior to turning on the shear field.[38−40] The shear field was imposed using a Couette cell, and the alignment of the lamellae was observed by in-situ small-angle neutron scattering. The scattering data were analyzed using a model that accounts for the granular nature (mosaic spread) of the aligned and unaligned microstructure.

Experimental Section

A nearly symmetric polystyrene−polyisoprene diblock copolymer was synthesized by anionic polymerization under high vacuum. The weight-average molecular weights of the polystyrene and polyisoprene blocks are 17.0 and 18.3 kg/mol, respectively, and we refer to this polymer as SI(17−18). The polydispersity index is 1.07. Polymer characterization methods are given in the ref 6. Experiments were conducted on a 51

wt % solution of SI(17−18) in distilled dioctyl phthalate (DOP). DOP is a nonvolatile solvent of polystyrene and polyisoprene. It is believed that the solvent is uniformly distributed throughout the sample. The plasticized polystyrene and polyisoprene microphases were well above their glass transition temperatures in the experimental temperature window (20−40 °C). No deuterium labeling was necessary due to the natural neutron contrast between polystyrene and polyisoprene. The volume fraction of polystyrene in the copolymer is 0.44. The quiescent order−disorder transition temperature of this solution, T_{ODT}, was measured by the local birefringence method[38,41,42] and found to be 29 ± 1 °C.

Measurements of small-angle neutron scattering (SANS) profiles under shear were carried out on the NG3 beam line at the National Institute of Standards and Technology (NIST) in Gaithersburg, MD. The Couette shear cell that we used was built by G. C. Straty at NIST in Boulder, CO. The scattering experiments and data reduction methods that we have used in this paper are identical to those used in an earlier paper.[19] We therefore only summarize the main points. The shear cell consists of two concentric quartz cylinders, an inner stator, and an outer rotor with inner diameter of 60 mm. The gap between the cylinders was 0.5 mm, and the motion of the rotor was controlled by a computer. A periodic shear field was imposed on the sample, where the time dependence of the rotor displacement had a triangular wave form. Following Koppi et al.,[7] we call this a reciprocating shear field. In all cases the strain amplitude was 400%. In the remainder of the paper, the shear field is specified by the frequency, ω (rad/s). The magnitude of the shear rate during each stroke of the reciprocating cycle is constant and equal to $4\omega/\pi$ (1/s). We used two instrument configurations, one where the beam was directed through the center of the cell, which we refer to as the radial configuration, and the other where the beam was directed through the edge of the cell, which we refer to as the tangential configuration. These configurations enable the measurement of scattering profiles in two planes: the scattering profile in the flow−vorticity plane was obtained in the radial configuration, while that in the velocity gradient−vorticity plane was obtained in the tangential configuration.

Neutrons with a wavelength λ of 0.6 nm were used with a vertical 1 mm × 12 mm slit as the sample aperture. The SANS intensity, normalized to a constant monitor count (10^8), was corrected for background scattering and was recorded as a function of $\mathbf{q}$, the scattering vector, $|\mathbf{q}| = 4\pi \sin(\theta/2)/\lambda$, where θ is the scattering angle. Two-dimensional SANS patterns were measured in 3−5 min intervals, using the following instrument configuration: wavelength spread, $\Delta\lambda/\lambda = 0.15$, sample-to-detector distance = 6.5 m, source-to-sample distance = 11 m, and source diameter = 2.7 cm. Scattering peaks or rings were located at $|\mathbf{q}| = q_{peak} = 0.27 \pm 0.01$ nm^{-1}, regardless of shear field and temperature. This indicates that in the ordered state (below 29 °C) the interlamellar spacing is 23 nm.[43]

Most of the scattered intensity was restricted to a ring defined by 0.22 (1/nm) ≤ $|\mathbf{q}|$ ≤ 0.34 (1/nm). This was found to be true regardless of temperature, shear field, and instrument configuration. Consequently, no information is lost when the data are converted to one-dimensional plots of the integrated intensity in the ring, 0.22 (1/nm) ≤ $|\mathbf{q}|$ ≤ 0.34 (1/nm), as a function of the azimuthal angle in the scattering plane. We use ϕ to denote the azimuthal angle in the velocity gradient−vorticity plane (tangential configuration) and ϕ_R to denote the azimuthal angle in the flow−vorticity plane (radial configuration). Both angles are measured with respect to the vorticity direction. The ring-averaged, radial and tangential scattering were normalized by the isotropic scattering extrapolated from the disordered state to account for differences in the scattering volume and average transmission coefficient in the two configurations.[19] The normalized tangential and radial scattering intensities are referred to as I and I_R, respectively. The normalizing factors for the tangential scattering profiles were 11.15 at 24 °C and 11.61 at 20 °C. The normalizing factor for the radial scattering profile at 24 °C was 47.21. This paper focuses on data obtained in the tangential configuration; all quantities without a subscript refer to the tangential configuration.

The grain structure of the sample under quiescent conditions was studied by depolarized light scattering.[38−40] The sample was held between optical flats with a path length of 1 mm. A HeNe laser with wavelength $\lambda = 632$ nm was used as the source, and the dependence of the depolarized scattering intensity on scattering vector, q ($q = 4\pi \sin(\theta/2)/\lambda$) where θ is the scattering angle) was measured with the help of a charged coupled device (CCD). In addition, the total forward depolarized scattering intensity at angles less than 14.6° was measured using a focusing lens as described in ref 33.

The rheological characterization of the SI(17−18)/DOP solution was carried out in a Rheometrics ARES melt state rheometer with 25 mm parallel plates, using a 200 g cm transducer with a lower sensitivity limit of 0.2 g cm, under a nitrogen atmosphere. The polymer solution was placed on the bottom plate, heated to 40 °C, and allowed to flow. Under these conditions, a bubble-free sample was obtained in less than half an hour. The top plate was then slowly brought in contact with the sample. The elastic and loss moduli (G' and G'', respectively) were measured at several temperatures between 23 °C (the lower limit of the instrument) and 45 °C. The strain amplitude was kept as low as possible to avoid shear-induced ordering and nonlinear viscoelastic responses. No evidence of shear-induced order was found during the rheological experiments. At 24.3 °C in the ordered state the strain amplitude ranged from 0.03% to 0.3%. Larger strains were used in the disordered state: at 30 °C in the disordered state the strain amplitude ranged from 0.1% to 10%, while at 45 °C, the strain amplitude ranged from 0.3% to 60%. The shear moduli at a given frequency and temperature were measured using at least two strain amplitudes. The acceptable strain amplitude range as a function of frequency and temperature was determined by ensuring that tan δ (tan $\delta = G'/G''$) was independent of strain amplitude. The reported rheological data, in the entire experimental range of frequencies and temperatures, were independent of strain amplitude; i.e., the measurements were made in the linear viscoelastic regime. For clarity, only one of the data sets is presented.

The shear alignment experiments were performed at two temperatures, 20.2 and 24.3 °C. Complementary depolarized light scattering experiments were conducted at 20.4 and 24.3 °C. The accuracy of the temperature control was ±0.2 °C. In the remainder of the paper we refer to the nominal temperatures of 20 and 24 °C.

Theory

In this section we develop a framework for neutron scattering from an ordered material comprising a collection of differently oriented lamellar grains. A grain is defined to be a region in the sample within which coherent order prevails. The scattering geometry and the nature of the ordered material are shown schematically in Figure 2. The structure at a given point $\mathbf{r}$ is characterized by a unit vector that points normal to the lamellae at that location. This vector, which is called the local director, is given the symbol $\mathbf{g}(\mathbf{r})$. We assume that the direction of $\mathbf{g}$ within each grain is sufficiently constant that the scattering from each such volume contributes coherently to the neutron scattering pattern. We can therefore express $\mathbf{g}(\mathbf{r})$ by the following expression:

$$\mathbf{g}(\mathbf{r}) = \sum_i \mathbf{g}_i f_i(\mathbf{r};\mathbf{g}_i) \tag{1}$$

where $\mathbf{g}_i$ is the optic axis of the ith grain and $f_i(\mathbf{r};\mathbf{g}_i)$ is the shape function for the ith grain, equal to unity if $\mathbf{r}$ is in the grain and 0 otherwise.

The geometry of the sample, in the tangential configuration, relative to the laboratory coordinate frame

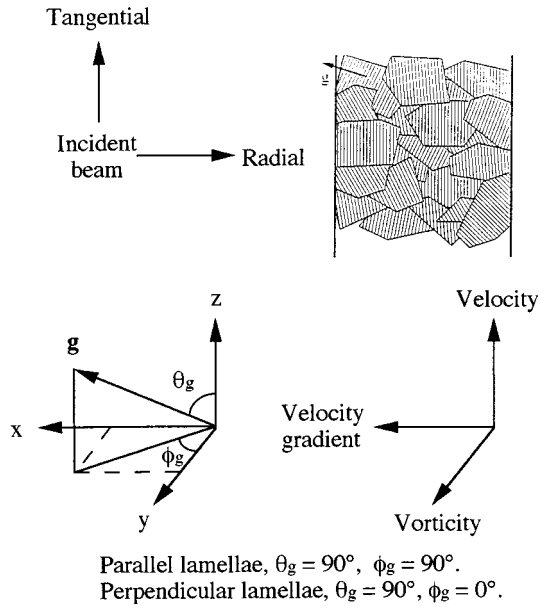

Figure 2. Schematic view of the scattering geometry and laboratory coordinate frame.

is depicted in Figure 2. A ray parallel to the incident neutron beam and tangent to the inner cylinder is taken as the z axis. A ray passing through the tangent point and directed toward the cylinder axis is the negative x axis. The y axis is taken to complete the right-handed orthogonal coordinate system. The velocity direction is parallel to the z axis along the plane $z = 0$. The velocity gradient at a point where $z = 0$ is directed along the x axis. The orientation of **g** with respect to the laboratory reference frame is defined by two angles: the angle between **g** and the z direction is θ_g, and the angle between the projection of **g** in the $x-y$ plane and the y direction is ϕ_g.

Within each grain the scattering length density, b, is assumed to have the following variation with **r**:

$$\delta b^2 = (b - b_{AV})^2 = \alpha \cos(2\pi \mathbf{r}\cdot\mathbf{g}/d) \tag{2}$$

where b_{AV} is the average scattering length density of the medium, d is the period of the lamellae, and α is proportional to the composition difference between adjacent lamellae. In terms of their polar angles, the unit vector along the optic axis, **g**, the unit vector, **s**, in the direction of the scattered wave, and the scattering vector, **q**, are given by

$$\mathbf{g} = \{\sin\theta_g \sin\phi_g, \sin\theta_g \cos\phi_g, \cos\theta_g\} \tag{3}$$

$$\mathbf{s} = \{\sin\theta_s \sin\phi_s, \sin\theta_s \cos\phi_s, \cos\theta_s\} \tag{4}$$

$$\mathbf{q} = k(\mathbf{s} - \mathbf{a}_z) = k\{\sin\theta_s \cos\phi_s, \sin\theta_s \sin\phi_s, \cos\theta_s - 1\} \tag{5}$$

where $k = 2\pi/\lambda$, and $\mathbf{a}_z$ is the unit vector along the z-axis.

The scattering profiles obtained from a collection of lamellar grains depend on the nature of the incident beam. The transverse coherence length of the incident beam, w_T, is determined by the degree of collimation[44] of the incident beam, and for our system $w_T \sim 240$ nm. This number characterizes the spatial coherence of the incident beam. The longitudinal coherence length, w_z, is due to the spread in wavelengths making up the incident neutron beam,[44] and for our system $w_z \sim 2.4$ nm. This number characterizes the temporal coherence of the incident beam. The effects of the individual coherence lengths on the neutron scattering profile are independent. For the present, we assume a monochromatic beam; when we refer to the degree of coherence, we mean spatial coherence. Later we will account for the effects of a spread in the distribution of wavelengths of the incident beam. If w_T is large compared to the transverse grain dimensions, the scattered profiles can be calculated as if w_T were infinite. In the opposite case, one may treat the transverse grain dimensions as effectively equal to w_T. We formulate the theory for these two limiting cases: case 1, a perfectly coherent incident beam; and case 2, the opposite limit where the transverse coherence length is short compared to the transverse grain dimensions.

Case 1: Perfectly Coherent Neutron Beam. For this case, the averaged scattered neutron flux per unit solid angle (or SANS intensity profile) in the single scattering limit (Born approximation) is proportional to

$$I(\mathbf{q}) = \int\int \sin\theta_g \, d\theta_g \, d\phi_g \, F(\theta_g,\phi_g) \int\int d\mathbf{r} \, d\mathbf{r}' \, C(\mathbf{r} - \mathbf{r}'; \mathbf{g}) \cos(2\pi\mathbf{r}\cdot\mathbf{g}/d) \cos(2\pi\mathbf{r}'\cdot\mathbf{g}/d) \exp(i\mathbf{q}\cdot(\mathbf{r} - \mathbf{r}')) \tag{6}$$

where $F(\theta_g,\phi_g)$ is the number of grains per unit solid angle whose **g** axis is centered at $\{\theta_g, \phi_g\}$, and the correlation function $C(\mathbf{r} - \mathbf{r}'; \mathbf{g})$ is the ensemble average of two-point products of shape functions for a given orientation of **g**:

$$C(\mathbf{r} - \mathbf{r}'; \mathbf{g}) = \sum_i \langle f_i(\mathbf{r};\mathbf{g}) \, f_i(\mathbf{r}';\mathbf{g}) \rangle \tag{7}$$

When we expand the cosine product in (6) using

$$\cos(2\pi\mathbf{r}\cdot\mathbf{g}/d) \cos(2\pi\mathbf{r}\cdot\mathbf{g}'/d) = \frac{1}{2}\cos(2\pi(\mathbf{r} - \mathbf{r}')\cdot\mathbf{g}/d) + \frac{1}{2}\cos(2\pi\,(\mathbf{r} + \mathbf{r}')\cdot\mathbf{g}/d) \tag{8}$$

the contribution of the second term to the integral is negligible because of its high spatial frequency and eq 6 becomes

$$I(\mathbf{q}) = \frac{1}{2} f V_{sample} \int\int \sin\theta_g \, d\theta_g \, d\phi_g \, F(\theta_g,\phi_g) \int d\mathbf{R} \times C(\mathbf{R};\mathbf{g})[\exp(i(\mathbf{q} + 2\pi\mathbf{g}/d)\cdot\mathbf{R}) + \exp(i(\mathbf{q} - 2\pi\mathbf{g}/d)\cdot\mathbf{R})] \tag{9}$$

where V_{sample} is the scattering volume of the sample, and f is the fraction of sample that is occupied by ordered grains. From eq 7 it follows that the correlation function is the probability that two points separated by the vector **R** are in the same grain. We assume forms for the correlation function that are sufficiently general to represent interesting physical cases, but of a simple enough mathematical form to allow for convenient models. Under quiescent conditions, that is in the absence of a shear field, the only preferred direction is along the director. The contours of constant probability are assumed to have the form of concentric ellipsoids of revolution with a common axis along the director:

$$C_{quiescent}(\mathbf{R};\mathbf{g}) = \exp\left(-\frac{(\mathbf{R}\cdot\mathbf{g})^2}{l_q^{\,2}}\right) \exp\left(-\frac{(\mathbf{R}\cdot\mathbf{m})^2 + (\mathbf{R}\cdot\mathbf{n})^2}{w_q^{\,2}}\right) \tag{10}$$

where $\{\mathbf{g},\mathbf{m},\mathbf{n}\}$ form a right-handed coordinate system, and the characteristic grain lengths along and perpendicular to the director are l_q and w_q, respectively.

In the presence of a shear field the symmetry of the quiescent case is lost. This may affect the contours of the correlation function in a particularly complicated way when the director makes a large angle with the $x-y$ plane. A tractable form for the correlation function can be recovered by exploiting the following fact: Because the Bragg resonances are sharp, the orientation of the directors that will contribute to the resonances are restricted to a small range of angles with respect to the z axis, i.e., $\theta_g \approx \pi/2$. When this is so, the second characteristic direction is the velocity direction, which is near the z axis. The remaining characteristic direction depends on ϕ_g and is perpendicular to these two directions. In general, the size parameters along these three directions are different. Thus, a reasonable form for the correlation function in the presence of shear is

$$C_{\text{shear}}(\mathbf{R};\mathbf{g}) = \exp\left(-\frac{(\mathbf{R}\cdot\mathbf{g})^2}{l_s^2}\right)\exp\left(-\frac{(\mathbf{R}\cdot\mathbf{m})^2}{w_{s1}^2}\right)\exp\left(-\frac{(\mathbf{R}\cdot\mathbf{n})^2}{w_{s2}^2}\right) \quad (11)$$

where, again, $\{\mathbf{g},\mathbf{m},\mathbf{n}\}$ form a right-handed coordinate system, and it is understood that the $\mathbf{m}$ direction corresponds to the velocity direction when $\mathbf{g}$ is in the $x-y$ plane. The grain structure under shear is thus characterized by three lengths: l_s, w_{s1}, and w_{s2}.

The correlation function describes the statistical properties of a collection of grains. Thus, the assumption of ellipsoidal correlation functions does not necessarily imply the presence of individual ellipsoidal grains (e.g., see schematic of grain structure in Figure 2).

For both quiescent and sheared states, the spatial integral in eq 9 is the contribution from grains with a particular $\mathbf{g}$ orientation:

$$\int d\mathbf{R}\, C(\mathbf{R};\mathbf{g})[\exp(i(\mathbf{q}+2\pi\mathbf{g}/d)\cdot\mathbf{R}) + \exp(i(\mathbf{q}-2\pi\mathbf{g}/d)\cdot\mathbf{R})] = \pi^{3/2} w_g w_m w_n \left[\exp\left(-\left(\mathbf{q}\cdot\mathbf{g}+\frac{2\pi}{d}\right)^2 \times \left(\frac{w_g^2}{4}\right)\right)\exp\left(-(\mathbf{q}\cdot\mathbf{m})^2\left(\frac{w_m^2}{4}\right)\right)\exp\left(-(\mathbf{q}\cdot\mathbf{n})^2\left(\frac{w_n^2}{4}\right)\right) + \text{term with } \frac{2\pi}{d} \to -\frac{2\pi}{d}\right] \quad (12)$$

where

$$\text{for } C = C_{\text{quiescent}}:\ w_g = l_q,\ w_m = w_n = w_q$$
$$\text{for } C = C_{\text{shear}}:\ w_g = l_s,\ w_m = w_{s1},\ w_n = w_{s2} \quad (13)$$

Scattering peaks, as a function of θ_g, ϕ_g, θ_s, and ϕ_s, will occur when the arguments of all three exponentials are equal to 0 in either of the terms on the right-hand side of eq 12. These peaks dominate the integrand when one evaluates the neutron flux from eq 9. The resonance scattering conditions are thus determined by

$$\mathbf{q} = \pm 2\pi\mathbf{g}/d \quad (14)$$

They are

$$\theta_{\text{Bragg}} = \cos^{-1}(\lambda/2d)$$
$$\theta_{g1} = \pi - \theta_{\text{Bragg}},\ \theta_{s0} = \pi - 2\theta_{\text{Bragg}},\ \phi_{s1} = \phi_g$$
$$\theta_{g2} = \theta_{\text{Bragg}},\ \theta_{s0} = \pi - 2\theta_{\text{Bragg}},\ \phi_{s2} = \phi_g + \pi \quad (15)$$

where $\{\theta_{s0}, \theta_{g1}, \phi_{s1}\}$ and $\{\theta_{s0}, \theta_{g2}, \phi_{s2}\}$ are the scattering and grain angle combinations that correspond to the resonance conditions.

We are interested in the behavior of the scattered intensity as we deviate from the resonance conditions, eq 15. If we expand the arguments of the exponentials in eq 12 in power series in the three variables $\{\theta_s, \theta_g, \phi_s - \phi_g\}$ and keep up to second-order terms, we get, for the range of parameters of interest, the accurate approximation consisting of a product of Gaussians:

$$\int d\mathbf{R}\, C(\mathbf{R};\mathbf{g})[\exp(i(\mathbf{q}+2\pi\mathbf{g}/d)\cdot\mathbf{R}) + \exp(i(\mathbf{q}-2\pi\mathbf{g}/d)\cdot\mathbf{R})] \approx \pi^{3/2} w_g w_m w_n \exp\left(-\left(\frac{\theta_s-\theta_{s0}}{\delta\theta_s}\right)^2\right) \times \exp\left(-\left(\frac{\theta_g-\theta_{g1}}{\delta\theta_g}\right)^2\right)\exp\left(-\left(\frac{\phi_s-\phi_g}{\delta\phi}\right)^2\right) + \left(\exp\left(-\left(\frac{\theta_s-\theta_{s0}}{\delta\theta_s}\right)^2\right)\exp\left(-\left(\frac{\theta_g-\theta_{g2}}{\delta\theta_g}\right)^2\right) \times \exp\left(-\left(\frac{\phi_s-\phi_g+\pi}{\delta\phi}\right)^2\right)\right) \quad (16)$$

where

$$\delta\theta_s = \frac{\lambda}{\pi w_g},\ \delta\theta_g = \frac{d}{\pi w_n},\ \delta\phi = \frac{d}{\pi w_m} \quad (17)$$

For either of the regimes, quiescent or shear, the values of the relevant correlation parameters are given by (13).

Case 2. Partially Coherent Neutron Beam. We account for the effects of the finite transverse coherence of the incident beam, w_T, by assuming that this length becomes the characteristic transverse dimension of the effective correlation function, independent of the orientation of the director. The characteristic length along the direction of the incident beam is called w_z. Thus, we use the effective correlation function

$$C(\mathbf{R}) = \exp\left(-\frac{Z^2}{w_z^2}\right)\exp\left(-\frac{X^2+Y^2}{w_T^2}\right) \quad (18)$$

where $\{X,Y,Z\}$ are the components of $\mathbf{R}$ in the frame tied to the direction of the incident beam. The scattered intensity is again given by eq 16, but now the angular widths of the resonance are

$$\delta\theta_s = \frac{\lambda}{\pi w_T},\ \delta\theta_g = \frac{d}{\pi w_z},\ \delta\phi = \frac{d}{\pi w_T} \quad (19)$$

Total Scattered Flux. Equations 9 and 16 indicate that a change in the scattering intensity along particular scattering directions $[I(\mathbf{q})]$ can be due to several factors: changes in the fraction of ordered material (f), the grain size parameters (w_g, w_m, w_n), or grain orientation $[F(\theta_g,\phi_g)]$. Additional complexity arises due to the interplay between the average grain dimension and coherence length of the neutron beam. It is thus difficult to identify the microstructural changes from observations based on $I(\mathbf{q})$, alone. It will be shown in this section

that some of these difficulties are alleviated when one considers changes in the total scattered flux.

We compute the total scattered flux for two conditions: (a) quiescent—a sample composed of randomly oriented grains, which leads to an azimuthally symmetric scattering profile in the plane perpendicular to the incident beam direction; and (b) shear-aligned—a sample composed of oriented grains wherein the grains have directors that vary in a restricted range about $\theta_g = 90°$, $\phi_g = 90°$. For both conditions the total scattered flux is given by

$$\text{total scattered flux} \propto \int\int \sin\theta_s \, d\theta_s \, d\phi_s \, I(\mathbf{q}) \quad (20)$$

For randomly oriented grains obtained under quiescent conditions, we take $F(\theta_g,\phi_g) = 1/(4\pi)$. Since the resonances are sharp, $\sin\theta_g \approx 1$, $\sin\theta_s \approx \lambda/d$, and evaluating the integral of the approximate form, eq 16, we get an expression independent of the correlation function parameters:

$$\text{total scattered flux} = (\text{constant})\pi^{-3/2} f_R V_{\text{sample}} \lambda^2 d \quad (21)$$

where f_R is the fraction of the sample volume occupied by randomly oriented grains.

For the shear-aligned grains case, we assume that all the grains are oriented uniformly over the conical solid angle $\Delta\Omega = \Delta\theta_g \Delta\phi_g$ centered at $\theta_g = 90°$, $\phi_g = 90°$ (tangential scattering from the parallel orientation). Thus, $F(\theta_g,\phi_g) = 1/(\Delta\theta_g\Delta\phi_g)$ and $\int d\phi_g \, F(\theta_g,\phi_g) = 1/\Delta\theta_g$, which gives

$$\text{total scattered flux} = (\text{constant})\pi^{-3/2} 2 f V_{\text{sample}} \lambda^2 d\left(\frac{1}{\Delta\theta_g}\right) \quad (22)$$

where f is the fraction of the sample volume occupied by aligned grains in the sheared sample.

If we define P_R to be the integrated scattered flux from a fully ordered sample comprising randomly oriented, aligned grains ($f_R = 1$) and P_S to be the integrated scattered flux from the same sample in the shear-aligned state, the ratio P_S/P_R is given by the ratio of the right-hand sides of eqs 21 and 22

$$\frac{P_S}{P_R} = \frac{\text{flux shear-aligned}}{\text{flux random}} = \frac{2f}{\Delta\theta_g} \quad (23)$$

Unlike $I(\mathbf{q})$, the ratio P_S/P_R is insensitive to a number of parameters such as the grain size and $\Delta\phi_g$ that must change during shear alignment. For the case when the shear field only reorients the grains in a fully ordered sample, i.e., $f = 1$, the change in P_S/P_R is equal to $2/\Delta\theta_g$.

Equation 23 assumes that the composition of the lamellae (δb) is unaffected by shear flow, and it therefore predicts that P_S/P_R should increase as shear alignment proceeds. However, it has been found that some systems undergo shear-induced disorder.[19] In this case the assumption of constant lamellar composition is invalid, and the ratio, P_S/P_R, will be given by a more general expression:

$$\frac{P_S}{P_R} = \frac{2f(\delta b/\delta b_e)^2}{\Delta\theta_g} \quad (24)$$

where δb is the scattering contrast between adjacent lamellae under shear, and δb_e is scattering contrast between adjacent lamellae under equilibrium, i.e., that obtained under quiescent conditions.

A noteworthy result of our analysis is that the total scattered flux is independent of the grain size parameters in the correlation function. In addition, we were able to represent the difference between coherent and partially coherent regimes entirely in terms of different parameters in the respective correlation functions. Thus, it is clear that the same expressions—eqs 23 and 24—derived for the case of perfect coherence also apply to partially coherent beams.

Effect of Finite Wavelength Spread ($\Delta\lambda$) on SANS

Our analysis thus far assumes a perfectly monochromatic beam. However, the neutron beam used in the experiments has a finite wavelength spread ($\Delta\lambda/\lambda = 0.15$). Thus, the incident beam is characterized by an incident flux per unit wavelength rather than simply an incident flux. The evaluation of the total scattered flux requires, beyond the procedures described above, an additional integral over the wavelength of the incident beam. If we assume that the fractional variation of the incident flux per unit wavelength is small over the width of the spectrum, $\Delta\lambda$, then the final integration simply yields the monochromatic result (at an intermediate wavelength) times a multiplicative constant proportional to the integrated power of the incident beam over all wavelengths.

Grain Structure Prior to Turning on the Shear Field

The ordering process under quiescent conditions was studied by depolarized light scattering.[38−40] The SI(17−18)/DOP solution was first disordered by annealing the sample at 41 °C for 40 min. This was done at the beginning of all experiments, to erase the effect of thermal and shear history and to ensure a uniform initial condition. The sample was then quenched into the ordered state (below 29 °C), and the depolarized light scattering intensity was measured as a function of time. We define time zero ($t = 0$) as the time at which the sample temperature was within 1 °C of the final temperature, which occurred 20 min after the temperature controller setting was switched.

The time dependence of the total depolarized light scattering in the range $0 < q < 2.56$ 1/μm for quenches to 20 and 24 °C is shown in Figure 3. At both quench temperatures, the signal begins to increase rapidly around $t \approx 0$, indicating the onset of order formation. At longer times, the ordering kinetics slow down considerably. These observations are consistent with previous work on ordering kinetics in block copolymers[33,34] where it was shown that the process occurred in two stages. In the early stage, grains grow rapidly by consuming the disordered phase. This continues until the entire sample is occupied by ordered grains. This is followed by a slow process where grains grow due to the annihilating of grain boundaries and other high free energy defects. The crossover from rapid grain growth to slow grain growth is thus an indication of the completion of the disorder-to-order transition. This crossover is clearly seen in Figure 3; at 24 °C, order formation requires 30 min, while at 20 °C, order formation requires 10 min. The light scattering signal

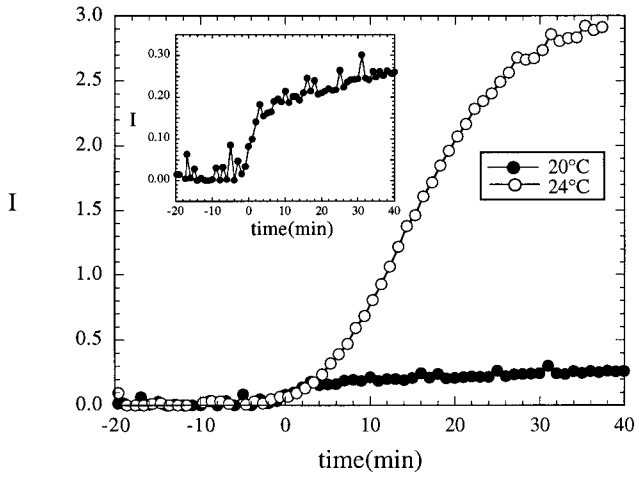

Figure 3. Time dependence of the total depolarized light scattering (I) from SI(17−18)/DOP after the quiescent quench to the 20 °C (solid circles) and 24 °C (hollow circles) from the disordered state. Inset: 20 °C data on an expanded scale.

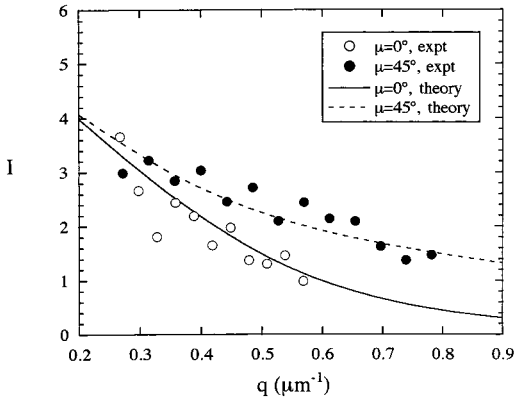

Figure 4. Angular dependence of the depolarized light scattering intensity from SI(17−18)/DOP, obtained at $t = 40$ min, after a quiescent quench from disordered state to 24 °C. The hollow and solid circles are the experimental data obtained at azimuthal angles of 0° and 45°, respectively. The lines are the theoretical fits from which we estimate grain dimensions.

at $t \approx 40$ min for the 24 °C quench is an order of magnitude larger than that at 20 °C. The scattering profile is related to the volume fraction of ordered grains (f_R) and the average grain size (l and w). Since $f_R = 1$ at $t \approx 40$ min in both cases, we conclude that grains formed at 24 °C are much larger than those formed at 20 °C.

We also measured the angular dependence of the depolarized light scattering intensity. The scattering intensity was measured as a function of scattering vector, q, and azimuthal angle in the scattering plane, μ, where $\mu = 0$ corresponds to the polarizer/analyzer axes. The scattering intensity $I(q,\mu)$ was obtained after subtracting the signal obtained from the sample in the disordered state, which we regard as background noise. The data obtained from the 24 °C quench at $t = 60$ min are shown in Figure 4 where we plot I versus q for $\mu = 0°$ and $\mu = 45°$. The scattering intensity along $\mu = 45°$ is larger than that along $\mu = 0°$, indicating the presence of anisotropic grains.[33,34] Anisotropic grains are expected due to the inherent anisotropy of ordered structures and have been observed in a variety of block copolymers.[33,34,44,45] As discussed in the Theory section, we characterize the grain structure by two length scales, l and w, where l is the correlation length in the direction

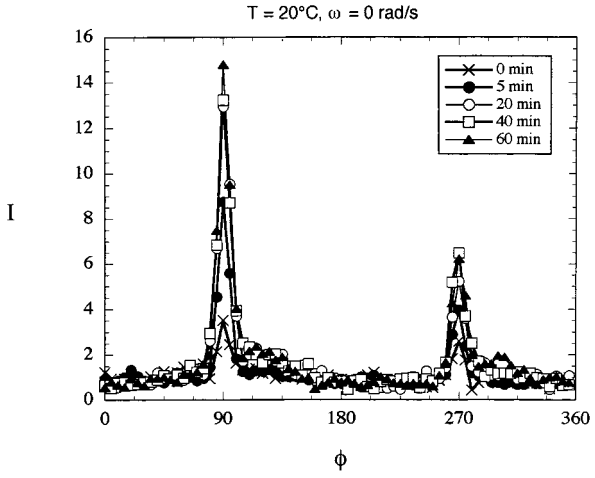

Figure 5. Evolution of the ring-averaged, tangential scattering intensity profile, $I(\phi)$, after a quiescent quench from the disordered state to 20 °C.

of lamellar normals and w is the correlation length in the two directions along the lamellae. Models that enable the determination of grain size from depolarized light scattering data are discussed in ref 33. The curves through the data in Figure 4 correspond to model calculations for ellipsoidal correlation functions with $l = 5.9$ μm and $w = 0.59$ μm, which minimizes the least squares of the deviations between theory and experiment. The average dimension of the grains at $T = 24$ °C and $t = 40$ min is 1.3 μm (geometric mean of l, w, and w).

The scattering signal at $t = 40$ min for the 24 °C quench is relatively weak (Figure 4) and close to the detection limit of our instrument. This is partly due to the fact that the grains obtained in this sample are relatively small. We tried to measure the angular dependence of the depolarized scattered light at $t = 40$ min during the 20 °C quench, but the signal was comparable to the signal obtained from the disordered sample. This is consistent with the total intensity measurements shown in Figure 3, which indicated that the average grain size obtained at 20 °C was much smaller than that obtained at 24 °C.

The total intensity measurements shown in Figure 3 can be used to estimate the grain size obtained during the 20 °C quench. In previous work it was shown that the integrated depolarized light scattering intensity from a fully ordered sample is proportional to the size of the grains, when the grains are much larger than the wavelength of light.[33] In Appendix 1, we extend this result to include cases where the grains are comparable in size to the wavelength of light. We estimate that the grains formed after ordering at 20 °C quench are smaller than those obtained at 24 °C by a factor of 0.267. The characteristic size of the grains after ordering at 20 °C is thus 0.35 μm.

In Figure 5 we show the normalized tangential SANS profiles, $I(\phi)$, obtained after a quiescent quench from the disordered state to 20 °C. The fact that I is dependent on ϕ indicates that quiescent cooling in our shear cell does not produce randomly oriented lamellae. The peaks at $\phi = 90°$ and 270° indicate the preference for obtaining lamellae in the parallel orientation. Similar scattering anisotropy was obtained at $T = 24$ °C. This tendency for obtaining parallel lamallae under quiescent conditions was also found in our previous experiments on SI/DOP solutions.[12,19]

We thus conclude that a quench from the disordered state to 20 and 24 °C in the SANS shear cell leads to a mixed state. A fraction of ordered grains are obtained in the parallel orientation while the remainder are randomly oriented. In a subsequent section, we show that this fraction is relatively small (13%). The depolarized light scattering signal is not sensitive to the presence of grains with parallel lamellae because the director of these grains is parallel to the propagation direction of the incident beam.[38] The depolarized light scattering analysis thus only pertains to the randomly oriented grains which occupy about 87% of the sample volume. This completes the characterization of the quiescent structure of the SI(17−18)/DOP sample, prior to turning on the shear field.

The protocols for studying the effect of shear on alignment were based on the results of the light scattering experiments. In the SD (shear disorder) experiments, the sample was quenched from the disordered state to either 20 or 24 °C in 20 min, and the shear field was imposed immediately ($t = 0$ in Figure 3). In the SO (shear order) experiments, the sample was quenched from the disordered state to either 20 or 24 °C in 20 min and held quiescently at that temperature for an additional 60 min, before turning on the shear field.

Rheological Characterization

The elastic and loss moduli (G' and G'', respectively) of the SI(17−18)/DOP solution in the disordered state (T > 30 °C) are shown in Figure 6a. Time−temperature superposition was used to obtain the master curve at a reference temperature of 30 °C. Both horizontal (a_T) and vertical (b_T) shifts were applied, and these are given in Table 1. The data in Figure 6a are reminiscent of an unentangled homopolymer melt.[45] The entanglement molecular weight (M_e) of polystyrene is 18 kg/mol, while that of polyisoprene is 5 kg/mol.[46] The addition of a solvent increases the effective M_e in accordance with a scaling law: $M_e \sim \phi_p^{-1.3}$, regardless of solvent quality (ϕ_p is the volume fraction of polymer).[47] The molecular weights of the polystyrene and polyisoprene chains for entanglement in a 51 wt % solution in DOP are thus 44 and 12 kg/mol, respectively. The molecular weight of the polystyrene block is thus below the entanglement threshold, while that of the polyisoprene block is above the entanglement threshold. It is therefore not entirely surprising that the viscoelastic properties of the disordered SI(17−18)/DOP solution resemble that of unentangled homopolymer melts.

The characteristic relaxation time of the chains, τ, is estimated to be equal to $(G'/\omega G'')_{\omega\to 0}$.[45] The data in Figure 6a indicate that $\tau = 0.122$ s at 30 °C. In Figure 6b we show that the temperature dependence of a_T is in good agreement with the familiar Williams−Landel−Ferry (WLF) equation. The straight line in Figure 6b enables us to obtain the temperature dependence of the molecular relaxation time:

$$\log a_T = \frac{\tau(s)}{0.122} = \frac{-10.42(T - 30.0)}{132.18 + T - 30.0} (T \text{ in } °C) \quad (25)$$

Our main aim is to characterize the SI(17−18)/DOP solution at the temperatures at which the shear alignment experiments were carried out, i.e., at 20 and 24 °C, which are in the ordered state. We assume that the rheological data obtained in the disordered state can be extrapolated to obtain estimates of τ in the ordered state. Experimental support for this assumption comes from the lack of a discontinuity in the chain self-diffusion coefficient at the order−disorder transition.[48,49] We thus use eq 25 to estimate τ in the ordered state, and the results are given in Table 1. The rheological characteristics of SI(17−18)/DOP solution, after the disorder-to-order process was completed at 24 °C, are displayed in Figure 6c where G' and G'' are plotted versus frequency (ω). Like other lamellar materials,[7−11] we observe approximate power law behavior for the frequency dependence of G' and G''. A single power law with an exponent of 0.64 applies to the G'' data over

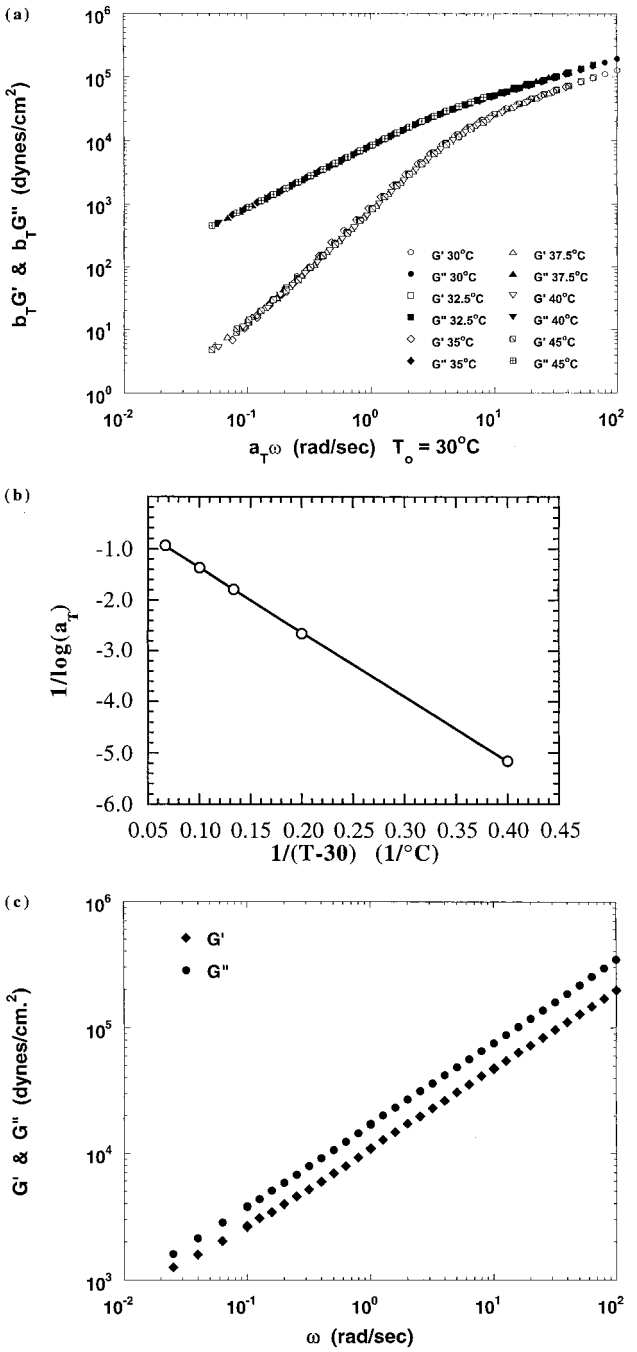

Figure 6. Rheological properties of the SI(17−18)/DOP solution. (a) Frequency dependence of G' and G'' in the disordered state at a reference temperature of 30 °C, using time−temperature superposition. (b) Temperature dependence of the horizontal shift factors, a_T, used to obtain the superposition shown in (a) and the WLF fit (line). (c) Frequency dependence of G' and G'' in the ordered state at 20 °C.

Table 1. Shift Factors Used To Obtain Time−Temperature Superposition of the Rheological Data in Figure 1a and Estimates of the Molecular Relaxation Times, τ, in the Disordered Fluid, Based on the Rheological Data[a]

temp (°C)	horizontal shift (a_T)	vertical shift (b_T)	relaxation time, τ (s)
45.0	0.084	0.90	0.011
40.0	0.185	0.91	0.023
37.5	0.275	0.93	0.034
35.0	0.420	0.95	0.051
32.5	0.640	0.98	0.078
30.0	1.00	1.0	0.122
24.4			0.353
20.2			0.833

[a] Estimates of τ at temperatures below 30 °C (in the ordered state) were obtained by extrapolating the WLF fit of for the temperature dependence of a_T.

the entire frequency range. The G' versus ω exponent changes slightly over the accessible frequency range; it is about 0.64 at high frequency and approaches 0.5 at low frequency. The rheological properties of the ordered phase were monitored for 50 min after the disorder-to-order transition was completed and found to be independent of time. It is evident that defect annihilation that is seen to occur during this time in the optical experiments (Figure 3) has no effect on rheology. This is consistent with previous studies on the effect of grain structure on rheology.[50]

Lamellar Alignment and Order Formation under Shear Flow

24 °C, ω = 0.63 rad/s. In Figure 7 we show the evolution of the tangential SANS profiles, $I(\phi)$, for the two shear alignment strategies SD (Figure 7a) and SO (Figure 7b) after a quench to 24 °C. The frequency of the reciprocating shear field, ω, was equal to 0.63 rad/s. Time zero for both the strategies is defined as the time at which the shear field is turned on. Both strategies lead to parallel lamellae, as indicated by the development of peaks at $\phi = 90°$ and 270°. It is evident that the peaks at $\phi = 90°$ and 270° are not of equal height. In Appendix 2, we show that this is due to path length differences of the scattered beams through the sample in the $\phi = 90°$ and 270° directions. This leads to a lower transmission coefficient for the $\phi = 270°$ beam. It is clear that the shape of the $I(\phi)$ data reflects the distribution of lamellar orientations. However, a detailed interpretation of the $I(\phi)$ data is not possible at this stage due to the multiplicity of effects that could lead to an increase in I at particular values of ϕ (see eqs 9 and 16). We therefore examine the evolution of the total scattered flux.

In Figure 8 we show the time dependence of I_{INT}, the integrated tangential SANS intensity, for SD and SO strategies for the 24 °C quench and $\omega = 0.63$ rad/s.

$$I_{INT} = \frac{1}{2\pi}\int_0^{2\pi} I(\phi_i)\, d\phi = \frac{P_S}{P_R} = \frac{2f}{\Delta\theta_g}$$

(if δb is not affected by shear) (26)

and

$$I_{INT} = \frac{2f(\delta b/\delta b_e)^2}{\Delta\theta_g}$$ (if δb is affected by shear) (27)

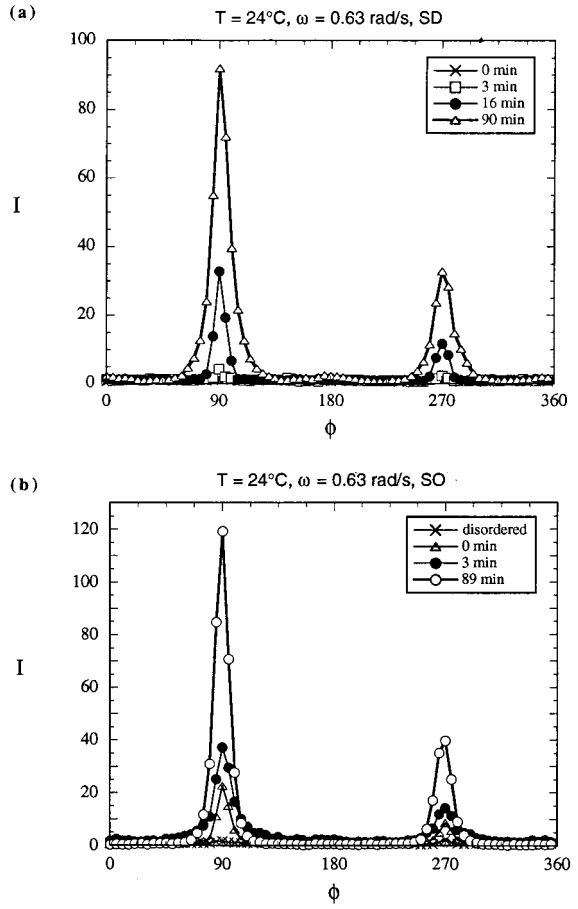

Figure 7. Evolution of the ring-averaged, tangential SANS intensity profile, $I(\phi)$, obtained from the two shear alignment strategies, SD (Figure 6a) and SO (Figure 6b), at 24 °C with $\omega = 0.63$ rad/s.

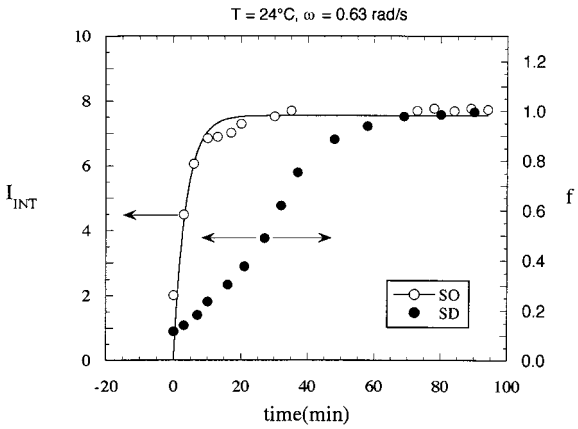

Figure 8. Integrated tangential SANS intensity, I_{INT}, as a function of time for SO (hollow circles) and SD (solid circles) experiments,with shearing rate 0.63 rad/s for the 24 °C quench. The solid line is an exponential fit through the SO data (see text). The right-hand y axis shows the time dependence of f, the volume fraction of ordered grains for the SD experiment.

We have normalized the scattering intensities so that the scattering produced by an isotropic arrangement of lamellar grains would be unity (see Experimental Section). We can thus equate I_{INT} to the ratio P_S/P_R introduced in eq 23 in the Theory section.

The application of shear flow, using both SD and SO strategies, leads to an increase in P_S/P_R (Figure 8). It is interesting to note that both strategies lead to the same

asymptotic value of about 8 at long times. If we assume that the sample is filled with ordered grains at long times ($f = 1$ at $t = 90$ min) for both SD and SO experiments, then, using eq 23, we conclude that $\Delta\theta_g$ is 2/8 rad or 14°. In Appendix 2 we show that this coincides with the instrument resolution limit of the tangential configuration. Since $\Delta\theta_g$ at long times is identical for the SD and SO protocol at $T = 24$ °C and $\omega = 0.63$ rad/s, we conclude that the quality of alignment, as judged by the integration of the tangential profiles upon completion of alignment, is independent of shear and thermal history. Note, however, that the tangential scattering profiles for the SD and SO strategies are different at $t \approx 90$ min (see Figure 7a,b). This indicates that the other parameters that characterize the sample, namely l, w, and $\Delta\phi_g$, depend on shear and thermal history. The peak intensity obtained under the SO protocol at 24 °C is somewhat higher than that with the SD protocol. In addition, the widths of the peaks, estimated by fitting the scattering data in the vicinity of $\phi = 90°$ to a Gaussian function [$I = I_0 \exp\{-(\phi - 90)^2/\Delta\phi_g^2\}$], are consistently larger during the SD protocol (e.g., at $t = 90$ min, $\Delta\phi_g = 10.1°$ for SD; $\Delta\phi_g = 8.3°$ for SO). These facts indicate that the SO protocol results in better alignment than the SD protocol at $T = 24$ °C and $\omega = 0.63$ rad/s.

The characteristic time of the alignment process during the SO strategy can be estimated by a least-squares fit of the $I_{INT}(t)$ data to the following functional form:

$$I_{INT} = I_{inf}[1 - \exp(-t/\tau)] \tag{28}$$

The solid curve through the SO data in Figure 8 is the least-squares fit to eq 28. This fit gives $I_{inf} = 7.54$ and $\tau = 3.7$ min. The characteristic time of alignment kinetics during the SO protocol is comparable to the time slices used for acquiring the SANS data, which was 3−5 min. The alignment kinetics are much slower during the SD protocol (Figure 8). It takes about 60 min for I_{INT} to reach a value of 7. Since T and ω are the same for both experiments, this difference must be due to the differences in the state of the sample at $t = 0$.

We consider two possible mechanisms for the rearrangement of randomly oriented grains during the SO experiments.[7−16] In the first mechanism, ordered grains with unfavorable orientations undergo an order-to-disorder transition in the presence of the shear field and then reappear in the preferred orientation. This is sometimes called the grain melting mechanism. In the second mechanism ordered grains simply rotate from their initial orientation to the preferred one. This is sometimes called the grain rotation mechanism. The time scale for restructuring in the SO protocol is 3−4 min, which is an order of magnitude smaller than the characteristic time for order formation under quiescent conditions (Figure 3, 24 °C data). If the shear field had caused an order-to-disorder transition, then the time scale for restructuring under the SO protocol would be comparable to the time scale for quiescent ordering at 24 °C, which is about 30 min. This is clearly not the case. Another possibility is that the time scale for conversion from disorder to order at 24 °C under reciprocating flow with $\omega = 0.63$ rad/s is very rapid with a time constant of 3−4 min. The SD protocol experiments enable a direct study of this process. These experiments indicted that at $T = 24$ °C and $\omega = 0.63$ rad/s the time scale for ordering kinetics was 60 min (Figure 8). We can thus rule out the grain melting mechanism under these conditions. We are forced to conclude that the alignment mechanism during the SO experiment at $T = 24$ °C and $\omega = 0.63$ rad/s must be grain rotation and that the characteristic time for grain rotation is 3−4 min or less.

It is reasonable to expect ordered grains that persist under shear flow to rapidly readjust their orientation so that $\Delta\theta_g \approx 0°$. It was shown by Leibler that the equilibrium lamellar spacing is dictated by a sharp minimum in the free energy.[43] The director of lamellar grains with $\Delta\theta_g \neq 0$ has a finite component along the flow direction. These lamellae must therefore undergo large changes in the lamellar spacing if they exist under flow. It has been argued that the high free energy of these states precludes the prolonged existence of such states under shear flow.[28,29,31] Only grains with $\Delta\theta_g = 0$ can preserve lamellar spacing under shear flow, and they therefore persist under flow.

Given the rapid kinetics of grain rotation, it is reasonable to assume that during the SD experiment all grains that form are such that $\Delta\theta_g \approx 0°$. In fact, during the early stages of the SD experiment, the ordered grains are surrounded by the disordered fluid, and so the kinetics of grain rotation will be even faster than that obtained during the SO experiment. Thus, even if grains form in nonparallel orientations during the SD experiment, we expect them to rotate rapidly so that $\Delta\theta_g \approx 0°$. It follows from eq 26 that I_{INT} during the SD protocol is proportional to f. Since $f \rightarrow 1$ at long times, we can say that at any time $f(t) \approx I_{INT}(t)/7.5$. The right-hand y-axis in Figure 8 shows the time dependence of f during the SD experiment. It is evident that it takes about 70 min for f to approach unity. This is comparable to the time required to complete the ordering process at $T = 24$ °C under quiescent conditions, which was about 40 min (see Figure 3).

During both SO and SD experiments, we observe the formation of perpendicular lamellae at intermediate stages of the alignment process. This is seen in Figure 9a where we show the tangential profile, $I(\phi)$, at $t = 11$ min for the SO experiment. The relatively broad peaks with a peak intensity of 4 units at $\phi = 0$ and 180° indicate the presence of perpendicular lamellae. The formation of perpendicular lamellae is seen more clearly in Figure 9b where the radial scattering profiles for the SO experiment at $t = 0$, 11, and 46 min are shown. Note the consistency in peak heights in the tangential and radial profiles at $t = 11$ min. An interesting unanswered question remains regarding the conversion of lamellae from the perpendicular to the parallel state. Does this happen by grain rotation or by melting? Unfortunately, at $T = 24$ °C and $\omega = 0.63$ rad/s, the scattering from the perpendicular lamellae is weak, and we cannot distinguish between these possibilities.

Since we can assume that $\theta_g \approx \theta_{g0} \approx 90°$ at all times under flow, the θ_g integrations in eqs 9 and 16 are irrelevant. In addition, the orientation distribution function of the lamellar grains under shear, $F(\theta_g,\phi_g)$, is only a function of ϕ_g, i.e., $F(\theta_g,\phi_g) = F(\phi_g)$. The characteristic grain sizes that we obtain under quiescent conditions are 1.3 and 0.35 μm at 24 and 20 °C, respectively. It is reasonable to assume that the grain dimensions under shear flow are larger than the grain dimensions obtained under quiescent conditions. Thus, grain sizes under flow are expected to be considerably larger than the transverse coherence length of the beam,

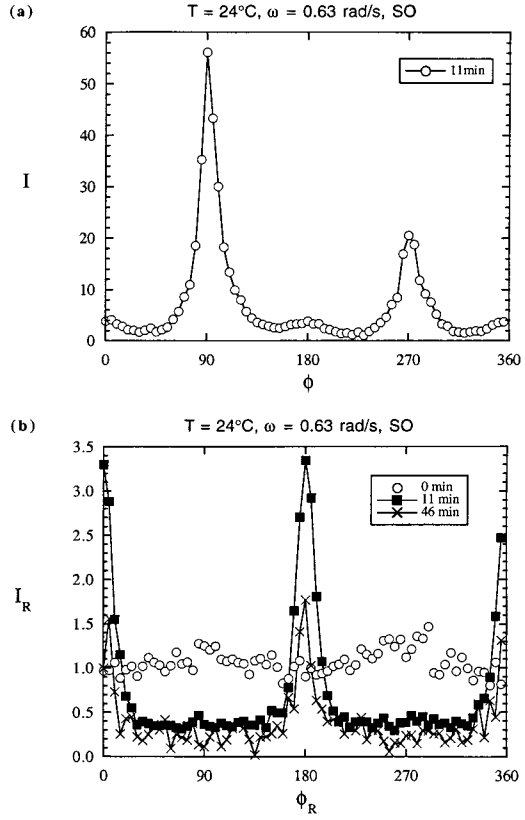

Figure 9. SANS profiles at selected times during the SO experiment at 24 °C with $\omega = 0.63$ rad/s: (a) tangential and (b) radial configuration.

which is 0.24 μm. It is therefore appropriate to use the results obtained for a partially coherent beam (eqs 9, 16, and 18). The measured SANS profiles are thus insensitive to grain size. The quantity $\delta\phi$ in eq 16 is about $1/10\pi$, which is an extremely small number. The Gaussian function in eq 16 with $\delta\phi$ in the argument can thus be regarded as a δ function. If we restrict our attention to scattering in the tangential instrument configuration, i.e., **q** is restricted to the velocity gradient−vorticity plane, then the above simplifications imply that

$$I(\phi) = (\text{constant})(\delta b)^2 f V_{\text{sample}} F(\phi_g = \phi) \qquad (29)$$

In the remainder of the paper, we focus on tangential scattering profiles which we use to quantify changes in f and $F(\phi_g)$: f is proportional to the magnitude of I_{INT}, and the shape of $F(\phi_g)$ is given by the ϕ dependence of I.

Summarizing the results thus far, at $T = 24$ °C and $\omega = 0.63$ rad/s, parallel lamellae are obtained at long times in both SD and SO experiments. We compare the alignment by comparing $\Delta\theta_g$ and $\Delta\phi_g$ at the end of the experiment. In both cases, $\Delta\theta_g \approx 0$ (i.e., $\Delta\theta_g$ is within instrumental resolution), but $\Delta\phi_g$ for SO protocol is smaller than that for the SD experiments. We conclude that under these conditions the SO protocol leads to better alignment.

20 °C. Figure 10 shows the evolution of the normalized tangential scattering with time at $T = 20$ °C, under shear flow with the SO strategy at $\omega = 0.63$ rad/s (Figure 10a), $\omega = 5.0$ rad/s (Figure 10b), and $\omega = 10.0$ rad/s (Figure 10c). In all three cases, we see a monotonic buildup of parallel lamellae as indicated by a monotonic

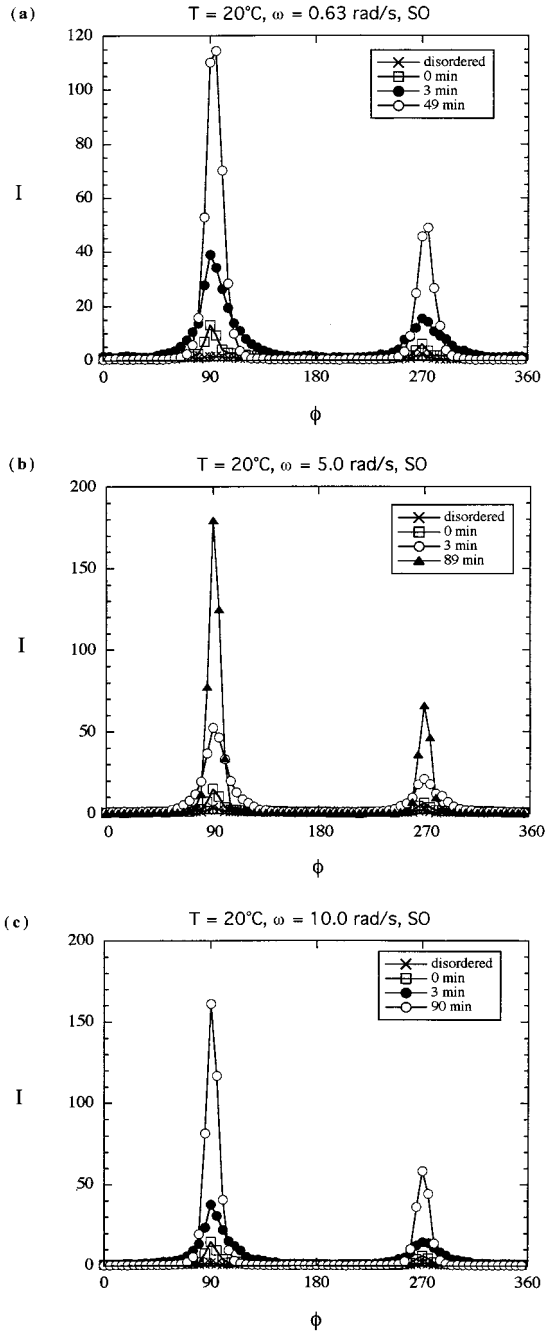

Figure 10. Evolution of the ring-averaged, tangential SANS intensity profile, $I(\phi)$, obtained at 20 °C, with the SO strategy at (a) $\omega = 0.63$ rad/s, (b) $\omega = 5.0$ rad/s, and (c) $\omega = 10.0$ rad/s.

increase in the scattering intensity at $\phi = 90°$ and 270°. This buildup is clearly seen in Figure 11a where the average peak intensity, I_{parallel} [$I_{\text{parallel}} = \{I(90°) + I(270°)\}/2$], is plotted versus time. In Figure 11b we show the time dependence of $I_{\text{perpendicular}}$ [$I_{\text{perpendicular}} = \{I(0°) + I(180°)\}/2$]. There is no evidence for the formation of perpendicular lamellae during the SO experiments.

The increase in I_{parallel} with time can be approximated by an exponential function [$I_{\text{parallel}} = I_{\text{inf}}(1 - \exp(-t/\tau))$]. The solid curves in Figure 11a represent least-squares fits through the data, which give $I_{\text{inf}} = 74$ and $\tau = 9.2$ min for $\omega = 0.63$ rad/s, $I_{\text{inf}} = 116$ and $\tau = 8.0$ min for $\omega = 5.0$ rad/s, and $I_{\text{inf}} = 108$ and $\tau = 11.8$ min for $\omega = 10.0$ rad/s. The peak width, $\Delta\phi_g$, is obtained by fitting

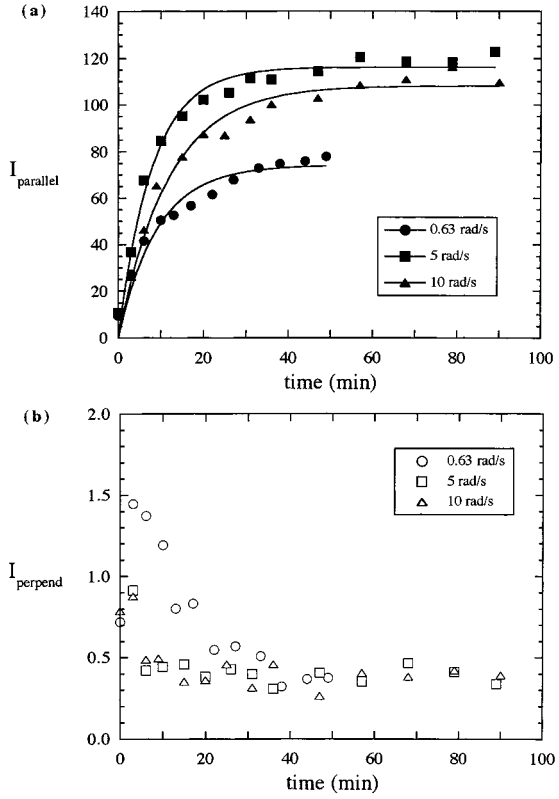

Figure 11. Time dependence of the average peak intensity along the principal directions accessible in the tangential configuration at 20 °C under the SO protocol with $\omega = 0.63$ rad/s (circles), $\omega = 5.0$ rad/s (squares), and $\omega = 10.0$ rad/s (triangles) during the SO experiment. (a) Intensity at $\phi = 90°$ and 270°, $I_{parallel}$, which is indicative of the concentration of grains with parallel lamellae. (b) Intensity at $\phi = 0°$ and 180°, $I_{perpend}$, which is indicative of the concentration of grains with perpendicular lamellae. The curves in Figure 10a are exponential fits through the data (see text).

the scattering data in the vicinity of the peak. At $t = 48 \pm 1$ min, $\Delta\phi_g = 10.0$ for $\omega = 0.63$ rad/s, $\Delta\phi_g = 7.2$ for $\omega = 5.0$ rad/s, and $\Delta\phi_g = 7.9$ for $\omega = 10.0$ rad/s. By all measures that are available to us ($I(t)$, I_{inf}, τ, and $\Delta\phi_g$), $\omega = 5$ rad/s appears to be optimal for obtaining a shear aligned sample at 20 °C. Note that the $I_{parallel}$ under this condition is 100 times larger than that obtained from the randomly oriented sample.

Figure 12 shows the evolution of the normalized tangential scattering with time under shear flow with the SD strategy at $\omega = 0.63$ rad/s (Figure 12a), $\omega = 5.0$ rad/s (Figure 12b), and $\omega = 10$ rad/s (Figure 12c). At all frequencies, we observe an increase in the scattering at $\phi = 0°$ and 180°, indicating a substantial buildup of perpendicular lamellae. The perpendicular lamellae coexist with parallel lamellae. For example, at $t = 3$ min and $\omega = 5$ rad/s we see four peaks at $\phi = 0°$, 90°, 180°, and 270° (see Figure 12b). The scattering peaks are not necessarily restricted to the vorticity and velocity gradient directions, as can be seen at $t = 20$ min and $\omega = 5.0$ rad/s (Figure 12b). These profiles have six peaks indicating the coexistence of three dominant orientations. According to eq 29, changes in $I(\phi)$ can be due to changes in f or $F(\phi_g)$. To isolate these effects, we examine the time dependence of the integrated tangential intensity (I_{INT}).

In Figure 13 we show $I_{INT}(t)$ for the SO and SD experiments at $T = 20$ °C. The data obtained under the SO protocol at 20 °C are virtually identical to those

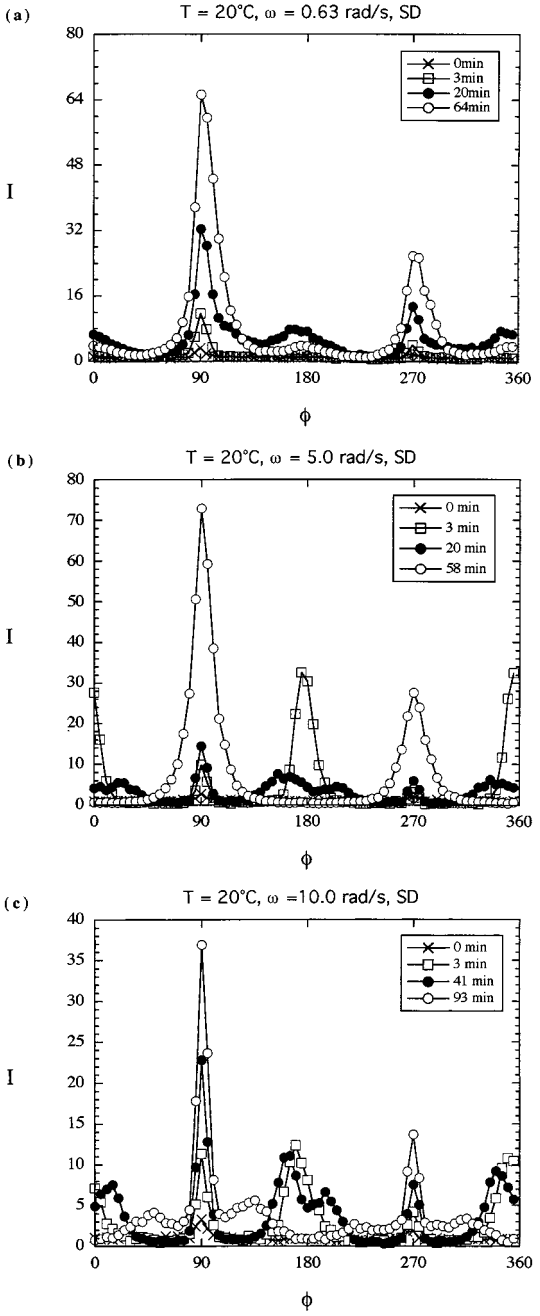

Figure 12. Evolution of the ring-averaged, tangential SANS intensity profile, $I(\phi)$, obtained at 20 °C, with the SD strategy at (a) $\omega = 0.63$ rad/s, (b) $\omega = 5.0$ rad/s, and (c) $\omega = 10.0$ rad/s.

obtained at 24 °C under the SO protocol (compare Figures 8 and 13, open symbols). We observe an exponential increase in I_{INT} [$I_{INT} = I_{inf}(1 - \exp(-t/\tau))$]. Exponential least-squares fits through the SO data at different shear frequencies give I_{inf} and τ that are very close to each other. To a good approximation $I_{inf} = 8.2$ and $\tau = 2.9$ min, regardless of ω. These estimates are similar to those obtained during the SO experiments at $T = 24$ °C. We had argued that at 24 °C the SO protocol resulted in rapid grain rotation so that $\Delta\theta_g \approx 0$. The same arguments apply to the SO experiments at 20 °C. We thus have evidence for rapid grain rotation under the SO protocol, regardless of temperature and shear frequency.

It is evident in Figure 13 (filled symbols) that the time dependence of I_{INT} during the SD experiments is quite

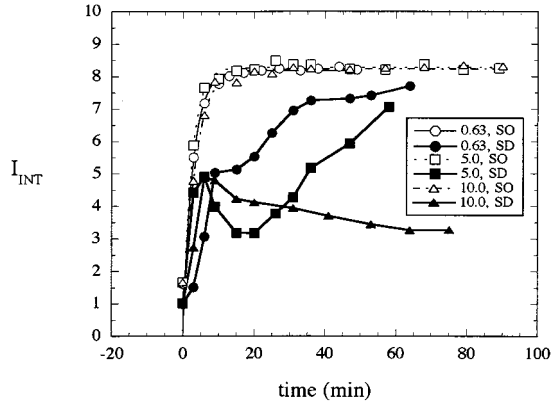

Figure 13. Integrated tangential SANS intensity, I_{INT}, as a function of time for SO (hollow symbols) and SD (solid symbols) experiments for the 20 °C quench. The curves through the hollow symbols are exponential fits through the SO data (see text). The solid symbols are connected by line segments for the sake of clarity.

complex. In all cases we see a sharp initial increase in I_{INT} which is similar to the initial changes seen in the SO experiments. An abrupt slowing down in the ordering kinetics is evident after I_{INT} reaches a value of about 5. Applying the ideas developed earlier, we can estimate f, the volume fraction of ordered material under flow prior to the slowing down, by calculating the ratio I_{INT}/I_{inf}. The shear-induced slowing down of the ordering kinetics is thus seen when $f \approx 0.6$, regardless of frequency. At $\omega = 0.63$ rad/s, the I_{INT} versus t gradient decreases dramatically at $t = 10$ min. At the higher frequencies (5 and 10 rad/s), the I_{INT} versus t gradient changes sign after f reaches 0.6. The decrease in I_{INT} with increasing time is a clear indication that some of the ordered grains in the sample undergo *shear-induced disorder*. Our measurements cannot distinguish between changes in δb, the scattering contrast between adjacent lamellae, and f, the volume fraction of the ordered phase (eq 27). One can argue that $|\delta b|$ must decrease during shear-induced disorder.

It is evident in Figure 12 that the populations of parallel lamellae increase monotonically with time because $I(\phi = 90°$ and $270°)$ increase monotonically with time. Thus, shear-induced disorder applies only to the transient, perpendicular lamellae. At $\omega = 5$ and 10 rad/s (Figure 12, b and c), we see that the peaks at $\phi = 90°$ and 270° split as they fade away. This is clearly seen at $t = 20$ min and $\omega = 5$ rad/s in Figure 12b and at $t = 41$ min and $\omega = 10$ rad/s in Figure 12c. This peak splitting was observed in a previous study, where it was established that this was a signature of an undulation instability.[19] This is shown schematically in Figure 14a. The lamellar orientation during the undulation instability is quantified by $\Delta\phi$, which is half the angle between the directors of adjacent grains.[51] In Figure 14b we show the time dependence of $\Delta\phi$ for $\omega = 5$ rad/s and $\omega = 10$ rad/s. One could view the increase in $\Delta\phi$ with time as direct evidence for grain rotation. The interesting feature is that the grain rotation is synchronous throughout the sample. The presence of six scattering peaks in Figure 12b,c indicates the presence of a well-defined, average orientation that is intermediate between perpendicular and parallel lamellae during the grain rotation process. At $\omega = 5$ rad/s, the increase in $\Delta\phi$ is relatively rapid, and the grain rotation process is completed in about 30 min. In contrast, at $\omega = 10$ rad/s, the grain rotation process is not complete even after

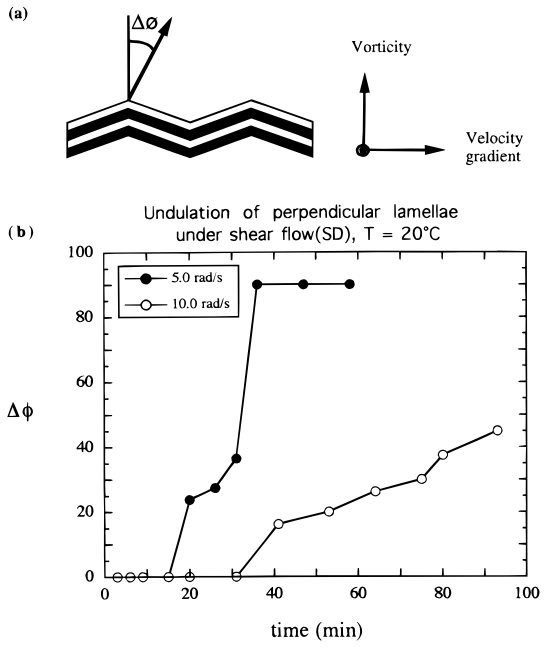

Figure 14. Undulation instability observed under the SD protocol at 20 °C. (a) A schematic view of undulating of perpendicular lamellae. The average angle between adjacent lamellar grains is $2\Delta\phi$. (b) The time dependence of $\Delta\phi$ at $\omega = 5.0$ and $\omega = 10.0$ rad/s.

90 min of shearing. It is evident in Figure 13 that $|\delta b|$ decreases during grain rotation. Hence, the mechanism for converting perpendicular to parallel lamellae is a combination of grain rotation (or undulation) *and* shear-induced disorder.

In Figure 15 we show the time dependence of $I_{parallel}$ and $I_{perpendicular}$ for the SD protocol at $\omega = 0.63$ rad/s (Figure 15a), $\omega = 5.0$ rad/s (Figure 15b), and $\omega = 10.0$ rad/s (Figure 15c). The transitory nature of the perpendicular lamellae is evident at all three frequencies. The population of parallel lamellae, gauged by the magnitude of $I_{parallel}$, continues to increase throughout the shear alignment process. At $\omega = 5$ rad/s, the increase in the population of grains with parallel orientation overwhelms the disordering of grains with perpendicular lamellae at $t > 35$ min. Beyond this point we see a continual buildup of order and indicated by a continuing increase in I_{INT} (Figure 13, filled squares). Note that at $\omega = 0.63$ and 5.0 rad/s I_{INT} approaches an asymptotic value of about 8 at long times (Figure 13). However, the fact that I_{INT} is somewhat less than 8 at the end of the shearing experiments (7.5 in the $\omega = 0.63$ rad/s case and 7 in the case of $\omega = 5.0$ rad/s) indicates that the ordering and alignment process was not completed even after 60 min of shearing.

At $\omega = 10.0$ rad/s, order formation under shear is severely suppressed. Even after 90 min of shearing we only see evidence for shear-induced disorder of perpendicular lamellae (Figure 13). However, the volume fraction of grains with parallel lamellae continue to increase (Figure 15c). It seems likely that at longer times the increase in the volume fraction of parallel lamellae will overwhelm the disordering of grains with perpendicular lamellae and give rise to a sample with parallel lamellae. This speculation is based on the observation that $dI_{parallel}/dt$ continues to increase with time in our experimental window (Figure 15c), suggesting that the state at much longer times will be the same as that obtained at 5 rad/s (Figure 15b). It thus appears

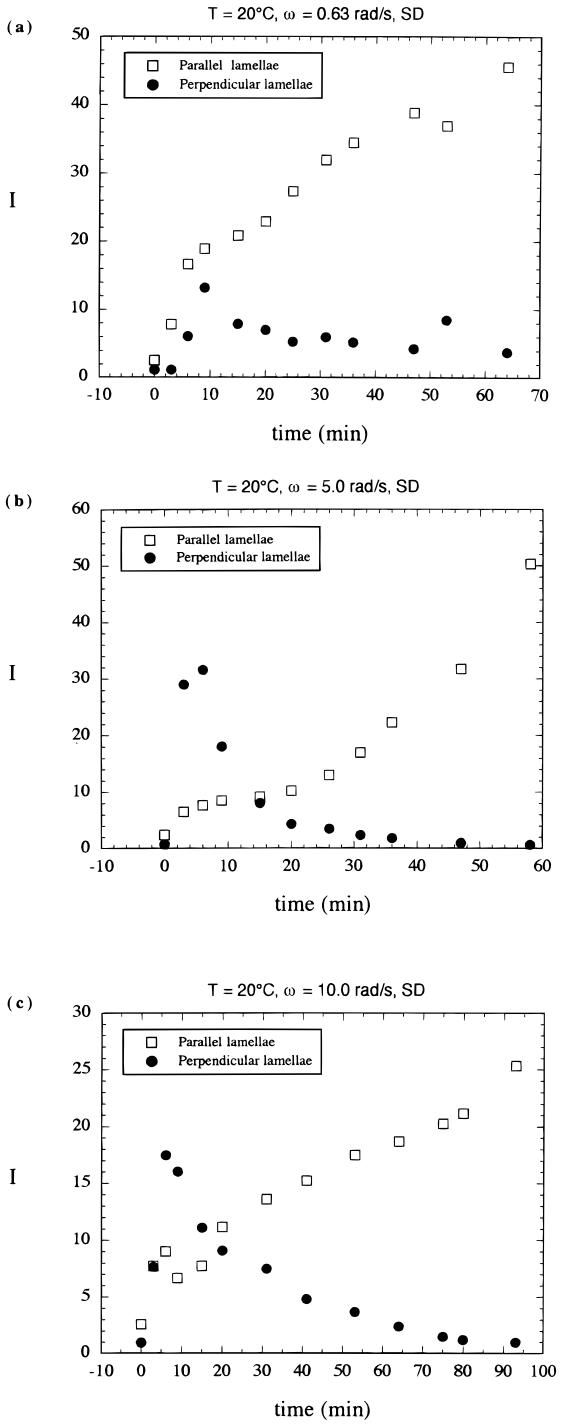

Figure 15. Time dependence of the average peak intensity along the principal directions accessible in the tangential configuration at 20 °C under the SD protocol at (a) $\omega = 0.63$ rad/s, (b) $\omega = 5.0$ rad/s, and (c) $\omega = 10.0$ rad/s.

that, regardless of frequency, the lamellae in our SI(17−18)/DOP solution under the SD protocol tend toward an all-parallel state at 20 °C.

We conclude this section by revisiting some of the issues discussed thus far. We found that I_{INT} at long times was about 8 ± 1 for all four SO experiments ($T =$ 24 °C, $\omega = 0.63$ rad/s; and $T = 20$ °C, $\omega = 0.63$, 5.0, and 10.0 rad/s) and for three out of four SD experiments ($T =$ 24 °C, $\omega = 0.63$ rad/s; and $T = 20$ °C, $\omega = 0.63$ and 5.0 rad/s). This consistency provides considerable support for our assumption that the sample is filled with ordered grains at long times, since it is highly unlikely that different thermal and shear histories would lead to the same partially ordered state. The values of I_{INT} obtained before starting shear flow in the SO experiments was about 2 (Figures 8 and 13). Assuming that the volume fraction of grains with parallel lamellae is f, and the remainder of the sample $(1 - f)$ is occupied by random grains, we obtain $f = (I_{INT} - 1)/8$. Thus, $f =$ 0.125; i.e., 12.5% of the sample volume is occupied by grains with parallel lamellae, and 87.5% of the sample is occupied by random grains before the shear flow was turned on in the SO experiments.

Our experiments provide evidence for the existence of a well-defined, aligned state that depends only on instantaneous temperature and frequency and is independent of sample history. In the SI(17−18)/DOP solution, this state happens to be parallel lamellae at all frequencies and temperatures that were examined. This implies that one could, in principle, construct phase diagrams of lamellar alignment as a function of temperature and frequency. However, the time required to obtain history-independent results was several orders of magnitude larger than the molecular relaxation time. In many block copolymer systems, achieving history-independent alignment phase diagrams may not be feasible.

Concluding Remarks

The effect of reciprocating shear flow on weakly ordered block copolymer lamellae was studied by in-situ small-angle neutron scattering. Our objective was to examine the development of order and alignment after the shear flow was turned on. We were particularly interested in distinguishing between transient intermediate states and long-time, steady-state behavior. We thus chose to conduct our study on a low-viscosity material: a solution of SI(17−18) and DOP with 51 wt % polymer. The molecular relaxation time of the polymer chains was 0.1−1 s, and the shear alignment studies were carried out for 60−90 min. The scattering data were analyzed using a model that accounted for the imperfect nature of the aligned state. We assumed that the sample was composed of coherently ordered grains whose statistical properties could be described by simple correlation functions. We studied the evolution of the grain orientation distribution function, $F(\theta_g,\phi_g)$, and the volume fraction of ordered grains, f. To our knowledge, quantitative analysis of scattering data under shear has not been attempted in any previous studies on block copolymer lamellae under shear. We varied sample temperature, reciprocating shear frequency, and the state of the sample prior to turning on the shear field: in one case, the shear field was turned on before significant ordering had taken place, i.e., shear flow was applied to a disordered sample (SD), while in the other, the shear field was turned on after the entire sample was filled with ordered grains (SO).

We found that the alignment pathways, i.e., the time dependence of $F(\theta_g,\phi_g)$ and f, was strongly influenced by the state of the system before turning on the shear flow. This was first reported by Zhang et al.[11] Aligned samples were characterized by $F(\theta_g,\phi_g)$ with peaks centered around $\theta_g = \theta_{g0}$ and $\phi_g = \phi_{g0}$ with widths $\Delta\theta_g$ and $\Delta\phi_g$, respectively (see Figure 2 for definitions). In the SO experiments, the early stages on alignment consisted of rapid grain rotation leading to $\theta_{g0} = 90°$. The characteristic time for grain rotation was compa-

rable to our resolution limit (3−4 min), regardless of temperature and frequency. This was followed by a somewhat slower grain rotation and/or defect annihilation which resulted in grains with both $\theta_{g0} = 90°$ and $\phi_{g0} = 90°$, i.e., the parallel alignment. The characteristic time of the slower process ranged from 8 to 10 min. The quality of the alignment ($\Delta\theta_g$ and $\Delta\phi_g$) after 60−90 min of shearing was dependent on temperature and frequency, but the final alignment (θ_{g0} and ϕ_{g0}) was not. In the SD experiments, the early stages consisted of a buildup of both parallel ($\phi_g = 90°$) and perpendicular ($\phi_g = 0°$) lamellae. This implies the existence of more complex distribution function, $F(\theta_g,\phi_g)$, with a multiplicity of peaks in ϕ_g. The perpendicular lamellae are transient in nature and eventually disappear via an undulation instability. We obtained clear evidence for shear-induced disorder during the undulation instability; i.e., the composition difference between adjacent lamellae weakens as they undulate. However, the buildup of parallel lamellae continues until the entire sample is filled with ordered grains with parallel lamellae. In all cases, the quality of alignment obtained in the SD experiments was much poorer than that obtained in the SO experiments. The kinetics of conversion of perpendicular to parallel lamellae are surprisingly slow. At $T = 20$ °C and $\omega = 10$ rad/s, this conversion is far from complete even after 90 min of shearing. The time scale for conversion of transient intermediate states to the "final" state under shear flow can be many orders of magnitude longer than the molecular relaxation time.

The alignment kinetics that we observed during the SD protocol appear to be related to the Deborah number, $De = \omega\tau$, where ω is the frequency of the shear field and τ is the molecular relaxation time. We conducted four SD shear-alignment experiments. In two cases we observed the formation of parallel lamellae via an undulation instability. The *De* for these experiments are 4.2 and 8.3. In the remaining two experiments, where no undulations were observed, *De* was 0.2 and 0.5. From the limited experiments conducted thus far it appears that the undulation instability occurs during the SD protocol when $De > 1$.

Our experiments indicate that it is best to turn on the shear field after the entire sample is filled with ordered grains, i.e., the SO protocol. In this case, the randomly oriented grains rotate on a time scale of about 3 min to give mostly parallel lamellae. For a given temperature, there appears to be an optimal frequency for obtaining the lowest defect density, i.e., the minimum value of $\Delta\phi_g$. At 20 °C we found that $\omega = 5$ rad/s was optimal. The rheological data from the ordered SI/DOP sample with randomly oriented grains showed no abrupt changes at $\omega = 5$ rad/s; see Figure 6c. There is thus no rheological fingerprint of the optimal shear alignment frequency. We note, however, that the optimum ω is roughly equal to $1/\tau$. It thus appears that the optimal frequency for shear alignment is in the vicinity of $1/\tau$. It is clear that choosing the optimal thermal (SO versus SD) and shear (ω) history is crucial for obtaining defect-free samples in a limited amount of time. Samples prepared under suboptimal conditions contain defects that are not easily annihilated by large-amplitude shear flow (e.g., Figures 11a and 13).

Our experiments demonstrate the importance of the initial state of the system prior to turning on the shear field, i.e., ordering kinetics under quiescent conditions. In addition, ordering kinetics under shear flow occur on a time scale that is somewhat slower than that obtained under quiescent conditions. Current theories[27−32] relate alignment in block copolymers to instantaneous shear rate and temperature. Our results indicate the need to extend these theories to account for the effects of shear and thermal history on alignment. The identification of universal features of shear alignment can only be made after such theories are developed. It is clear from our experiments that identifying the factors that govern the kinetics of ordering and alignment of block copolymers under shear flow is only possible after the factors that govern ordering kinetics under quiescent conditions are understood. Efforts to accomplish the latter are currently underway.[33−35,52−54]

Acknowledgment. We thank A. A. Lefebvre and M. Y. Chang for their help with this project. Financial support from the National Science Foundation (DMR-9457950), Research Corporation, and the Dreyfus Foundation to Polytechnic University is gratefully acknowledged. Acknowledgment is made to the donors of the Petroleum Research Fund, administered by the American Chemical Society, for support of this research. The SANS instrument at NIST[55] is supported by the National Science Foundation under Agreement DMR-9423101.

Appendix 1. Correction for Finite Lens Size in the Estimation of Grain Size from Integrated Depolarized Light Scattering

In earlier work[38−40] we had shown that the integrated depolarized light scattering flux could be used to estimate the average grain size, provided all the scattered light is collected and focused on the detector. As the grains become smaller, the angular spread increases to the point where this is not feasible. If a lens of radius R is used to focus the scattering from a sample located a distance L away from it, then the measured depolarized scattering power, P_m, is given by

$$\frac{P_m}{P_0} = \frac{4\pi^2}{15} f_R \Delta n^2 \frac{L_s l_{AV}}{\lambda^2}[1 - \exp\{-\pi(R l_{AV}/L\lambda)^2\}] \quad \text{(A1.1)}$$

where P_0 is the incident power, f_R is the fraction of the sample occupied by ordered grains, Δn is the difference in the refractive index of an ordered grain for light polarized parallel and perpendicular to the director, L_s is the sample thickness (path length), λ is the wavelength of the light, l_{AV} is the average grain size, R is the radius of the lens (30 mm), and L is the sample-to-lens distance (115 mm). Equation A1.1 was derived assuming that the grain structure could be described by a Gaussian correlation function, $C(r) = \exp(-r^2/w^2)$, and $l_{AV} = (2\pi)^{1/2}w$ (see refs 35 and 40 for details). For simplicity, we ignore the presence of two length scales in the correlation function at 24 °C and approximate $w = 1.3$ μm. We know that $P_m(24\ °C)/P_m(20\ °C) = 11.56$ at $t = 40$ min. Neglecting the temperature dependence of Δn, and solving eq A1.1, we get $w = 0.35$ μm.

Our analysis assumes the paraxial approximation which breaks down when $w/\lambda < 1/4$. It is thus clear that the paraxial approximation is valid for the grain structures studied in this work; $w/\lambda = 0.55$ for the smallest grains.

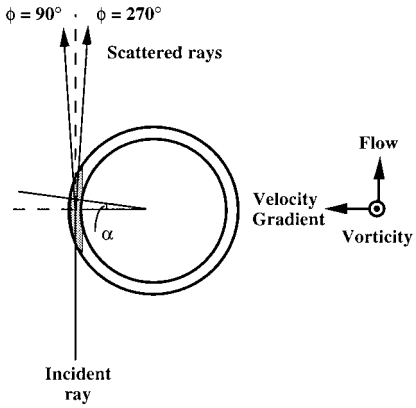

Figure 16. Schematic of the top view of the shear cell in the tangential configuration.

Appendix 2. Scattering from Parallel Lamellae in the Tangential Configuration

A schematic of the scattering geometry (top view) and the scattering volume is shown in Figure 16. If we assume perfect alignment of the lamellae along the walls of the shear cell, then the scattering contributions will be significant only when the lamellae satisfy the Bragg condition. The scattering angle is 1.48°. Thus, the lamellae corresponding to the $\phi = 90°$ ray are located at $\alpha = -0.74°$, while the lamellae corresponding to the $\phi = 270°$ ray are located at $\alpha = +0.74°$ (see Figure 16 for the definition of α). It turns out that the path length difference due to differences in α are negligible, and to a very good approximation we can assume that both rays originate at $\alpha = 0°$. From the geometry of the shear cell, it is easy to show that the path length for the $\phi = 90°$ ray is 3.19 mm while that for the $\phi = 270°$ ray is 4.76 mm. The measured transmission coefficient for a 1 mm thick SI(17−18)/DOP sample was 0.46. Using Beer's law, the transmission coefficient for the $\phi = 90°$ ray is 0.082 while that for the $\phi = 270°$ ray is 0.024. The ratio of the transmission coefficients is 3.4. This agrees well with observed anisotropy of the scattering profiles at $\phi = 90°$ and $\phi = 270°$ from a well-aligned sample which is in the vicinity of 3 (e.g., Figure 10b). The difference between 3 and 3.4 is probably due to stray reflections and empty cell scattering. These effects are difficult to quantify in the tangential geometry. When the lamellae are not aligned, the grains that obey Bragg's law are no longer localized at $\alpha = 0$, and this will lead to a lower scattering anisotropy. Note that when the quality of the alignment is relatively poor (e.g., Figure 10a), the observed scattering anisotropy is significantly lower than 3.

Simple geometry was used to determine that α corresponding to the edge of the scattering volume in Figure 16 is 12°. This limits the resolution with which $\Delta\theta_g$ can be measured to ±12° because a perfectly aligned sample with lamellae perfectly parallel to the shearing plates would not be perfectly parallel with respect to the laboratory coordinate frame.

Nomenclature

a_T	horizontal shift factor for superposition of rheological data
b_T	vertical shift factor for superposition of rheological data
b	scattering length density
b_{AV}	average scattering length density of the medium
C	correlation function
d	period of the lamellae
De	Deborah number
f	grain volume fraction
$f_i(\mathbf{r};\mathbf{g})$	shape function for the ith grain
f_R	volume fraction of randomly oriented, ordered grains
$F(\theta_g,\phi_g)$	fraction of grains per unit solid angle whose **g** vectors are centered at $\{\theta_g, \phi_g\}$
g	a unit vector along the optic axis
G'	elastic modulus
G''	loss modulus
I	normalized tangential SANS intensity
$I_{parallel}$	average peak intensity at 90° and 270° directions
$I_{perpendicular}$	average peak intensity at 0° and 180° directions
I_{inf}	integrated tangential SANS intensity at long times
I_{INT}	integrated tangential SANS intensity
I_R	normalized radial SANS intensity
$I(q)$	average scattered neutron flux
$I(q,\mu)$	depolarized light scattering intensity
l_{AV}	average grain size
l_q	characteristic grain length along the director
l_s	grain length along the director under shear
L_s	sample thickness (pass length)
M_e	entanglement molecular weight
q	scattering vector
r	vector from the origin to various points in the sample
P_R	integrated scattering power from a fully ordered sample comprising randomly oriented grains
P_S	integrated scattering power from the sample in the shear-aligned state
s	a unit vector in the direction of the scattered wave
SANS	small-angle neutron scattering
SD	shear flow acts on a disordered phase
SO	shear flow acts on an ordered phase
V_{sample}	volume of the sample
w	width of the grain
w_q	characteristic grain length perpendicular to the director
w_s	grain length perpendicular to the director under shear
w_T	transverse coherence length
w_z	longitudinal coherence length
δb	neutron scattering contrast between adjacent lamellae under shear
δb_e	neutron scattering contrast between adjacent lamellae under equilibrium
Δn	refractive index difference of an ordered grain for light polarized parallel and perpendicular to the lamellar normal
θ	scattering angle
θ_g	grain angle, the angle between local director g and velocity direction z
θ_{g0}	grain angle that correspond to the resonance condition
θ_{s0}	scattering angle that correspond to the resonance condition
λ	wavelength of incident radiation

τ	characteristic relaxation time
ϕ	azimuthal angle in the velocity gradient−vorticity plane (tangential configuration)
ϕ_g	azimuthal angle of **g** in the velocity gradient−vorticity plane
ϕ_R	azimuthal angle in the flow−vorticity plane (radial configuration)
ϕ_s	scattering angle in the velocity gradient−vorticity plane
ω	shear frequency in rad/s

References and Notes

(1) Paul, D. R., Newman, S., Eds. *Polymer Blends*; Academic Press: New York, 1978.
(2) Park, M.; Harrison, C.; Chakin, P. M.; Register, R. A.; Adamson, D. H. *Science* **1997**, *276*, 1401.
(3) Spatz, J. P.; Sheiko, S.; Moller, M. *Macromolecules* **1996**, *29*, 3220.
(4) Morton, M.; Fetters, L. J. *Rubber Chem. Technol.* **1975**, *48*, 359.
(5) Folkes, M. J.; Keller, A. *J. Polym. Sci., Polym. Phys. Ed.* **1976**, *14*, 833.
(6) Hadziioannou, G.; Skoulios, A. *Macromolecules* **1982**, *15*, 258.
(7) Koppi, K. A.; Tirrell, M.; Bates, F. S.; Almdal, K.; Colby, R. H. *J. Phys. (Paris)* **1992**, *2*, 1941.
(8) Patel, S. S.; Larson, R.; Winey, K. I.; Watanabe, H. *Macromolecules* **1995**, *28*, 4313.
(9) Gupta, V. K.; Krishnamoorti, R.; Kornfield, J. A.; Smith, S. D. *Macromolecules* **1995**, *28*, 4464.
(10) Chen, Z. R.; Issaian, A. M.; Kornfield, J. A.; Smith, S. D.; Grothaus, J. T.; Satkowski, M. M. *Macromolecules* **1997**, *30*, 7096.
(11) Zhang, Y.; Weisner, U.; Yang, Y.; Pakula, T.; Speiss, H. W. *Macromolecules* **1996**, *29*, 5427.
(12) (a) Balsara, N. P.; Hammouda, B. *Phys. Rev. Lett.* **1994**, *72*, 360. (b) Balsara, N. P.; Hammouda, B.; Kesani, P. K.; Jonnalagadda, S. V.; Straty, G. C. *Macromolecules* **1994**, *27*, 2566.
(13) Pinherio, D. B.; Winey, K. I. *Macromolecules* **1998**, *31*, 4447.
(14) Winter, H. H.; Scott, D. B.; Gronski, W.; Okamoto, S.; Hashimoto, T. *Macromolecules* **1993**, *26*, 7236.
(15) Almdal, K.; Bates, F. S.; Mortensen, K. *J. Chem. Phys.* **1992**, *96*, 9122.
(16) Morrison, F. A.; Mays, J. W.; Muthukumar, M.; Nakatani, A. I.; Han, C. C. *Macromolecules* **1993**, *26*, 5271.
(17) Balsara, N. P.; Dai, H. J.; Kesani, P. K.; Garetz, B. A.; Hammouda, B. *Macromolecules* **1994**, *27*, 7406.
(18) Balsara, N. P.; Dai, H. J. *J. Chem. Phys.* **1996**, *105*, 2942.
(19) Wang, H.; Kesani, P. K.; Balsara, N. P.; Hammouda, B. *Macromolecules* **1997**, *30*, 983.
(20) Nakatani, A. I.; Morrison, F. A.; Douglas, J. F.; Mays, J. W.; Jackson, C. L.; Muthukumar, M.; Han, C. C. *J. Chem. Phys.* **1996**, *104*, 1589.
(21) Tepe, T.; Schulz, M. F.; Zhao, J.; Tirrell, M.; Bates, F. S. *Macromolecules* **1995**, *28*, 3008.
(22) Koppi, K. A.; Tirrell, M.; Bates, F. S. *Phys. Rev. Lett.* **1993**, *70*, 1449.
(23) Hajduk, D. A.; Tepe, T.; Takenouchi, H.; Tirrell, M.; Bates, F. S.; Almdal, K.; Mortensen, K. *J. Chem. Phys.* **1998**, *108*, 326.
(24) Ackerson B. J.; Clark, N. A. *Physica* **1983**, *118A*, 221.
(25) Ramaswamy, S. *Phys. Rev. Lett.* **1992**, *69*, 112.
(26) Safinya, C. R.; Sirota, E. B.; Bruinsma, R. F.; Jeppesen, C.; Plano, R. J.; Wenzel, L. J. *Science* **1993**, *261*, 588.
(27) Bruinsma, R. F.; Safinya, C. R. *Phys. Rev. A* **1991**, *43*, 5377.
(28) Cates, M. E.; Milner, S. T. *Phys. Rev. Lett.* **1989**, *62*, 1856.
(29) Cates, M. E.; Marques, C. M. *J. Phys. (Paris)* **1990**, *51*, 1733.
(30) Huang, C. Y.; Muthukumar, M. *J. Chem. Phys.* **1997**, *107*, 5561.
(31) Fredrickson, G. H. *J. Rheol.* **1994**, *38*, 1045.
(32) Goulian, M.; Milner, S. T. *Phys. Rev. Lett.* **1995**, *74*, 1775.
(33) Newstein, M. C.; Garetz, B. A.; Balsara, N. P.; Chang, M. Y.; Dai, H. J. *Macromolecules* **1998**, *31*, 64.
(34) Dai, H. J.; Balsara, N. P.; Garetz, B. A.; Newstein, M. C. *Phys. Rev. Lett.* **1996**, *77*, 3677.
(35) Balsara, N. P.; Garetz, B. A.; Chang, M. Y.; Dai, H. J.; Newstein, M. C.; Goveas, J.; Krishnamoorti, R. Rai, S. *Macromolecules* **1998**, *31*, 5309.
(36) Hajduk, D. A.; Takenouchi, H.; Hillmyer, M. A.; Bates, F. S.; Vigild, M. E.; Almdal, K. *Macromolecules* **1997**, *30*, 3788.
(37) This is based on extrapolations of the rheological data on the disordered fluid. The rheology of the ordered material is complex, and the physical underpinnings of these data are not understood.
(38) Balsara, N. P.; Garetz, B. A.; Dai, H. J. *Macromolecules* **1992**, *25*, 6072.
(39) Garetz, B. A.; Balsara, N. P.; Dai, H. J.; Wang, Z.; Newstein, M. C.; Majumdar, B. *Macromolecules* **1996**, *29*, 4679.
(40) Garetz, B. A.; Newstein, M. C.; Dai, H. J.; Jonnalagadda, S. V.; Balsara, N. P. *Macromolecules* **1993**, *26*, 3151.
(41) Amundson, K. R.; Helfand, E.; Patel, S. S.; Quan, X.; Smith, S. S. *Macromolecules* **1992**, *25*, 1953.
(42) Balsara, N. P.; Perahia, D.; Safinya, C. R.; Tirrell, M.; Lodge, T. P. *Macromolecules* **1992**, *25*, 3896.
(43) Leibler, L. *Macromolecules* **1980**, *13*, 1602.
(44) The scattering analysis assumes an infinitely coherent incident beam. According to a private communication from Charlie Glinka of NIST, Gaithersburg, MD, the spatial coherence of neutron beams produced in nuclear reactors is not a completely resolved issue. The transverse coherence is estimated to λ/(angle subtended by source at sample). The longitudinal coherence (in the propagation direction) is estimated to be $\lambda^2/\Delta\lambda$.
(45) Ferry, J. *Viscoelastic Properties of Polymers*, 3rd ed.; Academic Press: New York, 1980.
(46) Fetters, L. J.; Lohse, D. J.; Colby, R. H. In *Physical Properties of Polymers Handbook*; Mark, J. E., Ed.; AIP Press: Woodbury, NY, 1996; Chapter 24.
(47) Colby, R. H.; Fetters, L. J.; Funk, W. G.; Graessley, W. W. *Macromolecules* **1991**, *24*, 3873.
(48) Shull, K. R.; Kramer, E. J.; Bates, F. S.; Rosedale, J. H. *Macromolecules* **1991**, *24*, 1383.
(49) Balsara, N. P.; Stepanek, P.; Lodge, T. P.; Tirrell, M. *Macromolecules* **1991**, *24*, 6227.
(50) Balsara N. P.; Dai, H. J.; Watanabe, H.; Sato, T.; Osaki, K. *Macromolecules* **1996**, *29*, 3507.
(51) The drawing in Figure 13a is a simplified view of reality, because if this were the case, then we would obtain four resolution-limited peaks at $\phi = 90° \pm \Delta\phi$ and $270° \pm \Delta\phi$. The finite width of the four peaks indicates that the lamellar planes under go smooth undulations rather than the abrupt buckling shown in Figure 13a.
(52) Hajduk, D. A.; Tepe, T.; Takenouchi, H.; Tirrell, M.; Bates, F. S.; Almdal., K.; Mortensen, K. *J. Chem. Phys.* **1998**, *106*, 326.
(53) Sakamoto, N.; Hashimoto, T. *Macromolecules* **1998**, *31*, 3815.
(54) Balsara N. P.; Garetz, B. A.; Newstein, M. C.; Bauer, B. A.; Prosa, T. *Macromolecules* **1998**, *31*, 7668.
(55) Certain equipment and instruments or materials are identified in this paper in order to adequately specify the experimental details. Such identification does not imply recommendation by the National Institute of Standards and Technology, nor does it imply the materials are necessarily the best available for the purpose.

MA981226D